THESIS FOR THE DEGREE OF DOCTOR OF PHILOSOPHY

From single-molecule sensing to extracellular vesicles in glioma cells under stress

Virginia Claudio

Department of Applied Physics
CHALMERS UNIVERSITY OF TECHNOLOGY
Göteborg, Sweden 2017

From single-molecule sensing to extracellular vesicles in glioma cells under stress
Virginia Claudio
ISBN 978-91-7597-591-7

Doktorsavhandlingar vid Chalmers tekniska högskola
Ny serie nr 4272
ISSN 0346-718X

Department of Physics
Chalmers University of Technology
SE-412 96 Göteborg
Sweden
Telephone +46 (0)31 772 1000

Chalmers Reproservice
Göteborg, Sweden 2017

To Ella

From single-molecule sensing to characterization of extracellular vesicles in glioma cells under stress

Virginia Claudio
Department of Applied Physics
Chalmers University of Technology

Abstract

This thesis describes the work I conducted in two different areas, namely biomolecular sensing and quantitative cell biology. The work in the former area was focused on the optimization of plasmonic metamaterials for sensing applications, and in the latter on the characterization of extracellular vesicles released by glioblastoma cells under stress conditions. If these two areas appear to be very far apart, it is because they are; however, they are not entirely disconnected. Understanding the biological function of extracellular vesicles depends on the information that can be obtained using bioanalytical sensors, which consequently relates to the information that can be gained from cellular experiments. Attempts were therefore made to review and exploit biophysical approaches that link the two areas, with focus on how detailed insights about the nature of these vesicles relate to their biological function.

At its core, this thesis deals with: i) plasmonic biomolecular sensing, discussing noise-related issues, single-molecule detection and a dual-wavelength method to extract more – and more accurate – information from ensemble measurements of complex macromolecular entities, including extracellular vesicles; ii) an introduction to glioblastomas, cellular models of hypoxic and oxidative stress, the role of extracellular vesicles in cellular communication in cancer, and an exploratory omics approach to understand how the biochemical composition of cells and vesicles changes across different cell lines in response to stress. As an encompassing bridge, a review on the techniques used to characterize extracellular vesicles also acts as an integrating element of this thesis and will help the reader understand different aspects of relevance with respect to how the physical and biological viewpoints intersect.

The main findings of the work on biomolecular sensing consist in: i) the clarification of the interplay between inhomogeneous binding probability to a nanosensor (which depends on diffusion/geometry) and the inhomogeneous sensitivity distribution of the nanosensor itself as combined sources of detection uncertainty and ii) a method exploiting dual-wavelength plasmonic sensing to estimate the degree of deformation of adsorbed extracellular vesicles and hence more accurate determination of their mean size and bulk concentration. In the second area we find that iii) the proteome of vesicles mainly depends on cell type of origin and is greatly affected by stress, although in a heterogeneous way, with respect to the cells proteome; on the contrary, iv) the lipid composition of extracellular vesicles is very stable across cell types and stress.

Keywords: single molecule sensing, surface plasmon resonance, nanoplasmonics, extracellular vesicles, exosomes, cellular stress, glioblastoma, proteome, lipid composition.

APPENDED PAPERS

The thesis is based on the following papers:

Paper I

A simple model for the resonance shift of localized plasmons due to dielectric particle adhesion

Tomasz J. Antosiewicz, Peter S. Apell, Virginia Claudio, Mikael Käll

Optics Express, 2012, (20) 1, 524-533

Paper II

Single-particle Plasmon sensing of discrete molecular events: binding position versus signal variations for different sensor geometries

Virginia Claudio, Andreas B. Dahlin, Tomasz J. Antosiewicz

The Journal of Physical Chemistry C, 2014, 118 (13), 6980-6988

Paper III

Dual-Wavelength Surface Plasmon Resonance for Determining the Size and Concentration of Sub-Populations of Extracellular Vesicles

Deborah L. M. Rupert, Ganesh. V. Shelke, Gustav Emilsson, Virginia Claudio, Stephan Block, Cecilia Lässer, Andreas B. Dahlin, Jan O. Lötvall, Marta Bally, Vladimir P. Zhdanov, Fredrik Höök

Analytical chemistry, 09/2016, 88(20)

Paper IV

Methods for the physical characterization and quantification of extracellular vesicles in biological samples

Deborah L. M. Rupert, Virginia Claudio, Cecilia Lässer, Marta Bally

Biochimica et Biophysica Acta (BBA) - General Subjects 08/2016; 1861(1)

Paper V

Extracellular vesicles from glioma stem cells show cell line-specific proteomes and mainly heterogeneous response to stress

Virginia Claudio, Ágota C. Tüzesi, Wojciech Michno, Chesia Testa, Prince N. Twum, Jörg Hanrieder, Helena Carén, H. Georg Kuhn

In manuscript

CONTRIBUTIONS TO APPENDED PAPERS

Paper I

I contributed to the discussion.

Paper II

I set up the model and implemented the work. I analyzed the data and wrote the manuscript.

Paper III

I contributed to the discussion and the analysis of the dual-wavelength SPR data.

Paper IV

I was actively involved in the planning and writing of the review article. Specifically, I contributed to the manuscript with knowledge related to the biomolecular identity of extracellular vesicles and to the methods for the characterization of their biomolecular profile.

Paper V

I set up the methods and models, designed and conducted the experiments. I performed the data analysis and interpretation. I wrote the manuscript.

Contents

Chapter 1
Introduction

In 2001 the National Institute of Health released a detailed program announcement encouraging basic research on the detection and manipulation of single molecules [1]. This and other ongoing large scale efforts are motivated by the limitations associated with ensemble experiments where details on the molecular properties are lost in the averaging. Moreover, reaction dynamics are hard to determine when the concentration of interacting molecular species is low and sensitivity is poor. In comparison, an incredible amount of chemical, biological and medical information can be uncovered by single-molecule investigations [2]–[4].

The variety of techniques available to measure molecular forces, structure, electronic states and interactions with other molecules is astonishing. The most versatile and the least perturbing methods are light-based. For instance, fluorescence in all its flavors dominates *in vivo* cellular studies revealing the mechanisms of protein-protein interactions, molecular motors, and all sorts of dynamic behaviors [5], [6]. Optical forces can also be used to trap and manipulate nano-objects, including molecules [7], [8]. Single-molecule sensitivity is the ultimate goal in clinical applications such as the detection and quantification of disease markers and novel drug screening methods [9]–[11].

In the past two decades many advances have been made to further the development of high resolution sensing schemes and the understanding of microscopic molecular behavior, however it is still rather uncommon to see single-molecule assay platforms in large-scale use. This is mainly due to the obstacles of parallelization and set-up robustness. On the way to finding new technological solutions, plasmonic sensing is seen as one of the strongest candidates for achieving multiplexed single-molecule real-time and label-free detection. To this day, we have the proof of some of the above-mentioned features, though not all at once in a single set-up. However, several questions still remain unanswered, leaving room for optimization and new ideas.

At the same time medical and biological research has been uncovering interesting and promising functions of sub-micron-sized particles shed by cells and called extracellular vesicles, with particular emphasis on one type called exosomes. In addition and as a complement to their biological characterization, the physico-chemical properties of native vesicles are of great importance to the study of cellular communication in normal and disease states. Such knowledge can also be used for the development of artificial vesicles that can interact in an effective and tailored fashion with the intended recipient cells.

Here multiple disciplines intersect to explore the complexity of biological material and the system-wide effects that unknown amounts of these tiny heterogeneous entities have on the whole living organism.

One prominent example of the role of extracellular vesicles in cellular communication is the case of cancer. Tumor cells have been found to release greater amounts of extracellular vesicles than their normal counterpart and therefore are well-suited to produce and characterize these vesicles in vitro.

In this thesis work I have combined physical and biological research.

In Ch. 2 I attempt to give an overview of the basic biology of one type of cancer cells and what extracellular vesicles are.

I illustrate in Ch. 3 the basics of cellular stress models of cancer and how extracellular vesicles play a role in "informing" the environment about the changes that cells may undergo locally in response to a stress stimulus. Also, initial experiments to detect cellular stress in our model system are reported.

Ch. 4 outlines general aspects of surface-based sensing, including the sources of noise and uncertainty in few molecule measurements.

Ch. 5 summarizes the basics of plasmonic sensing, focusing on two distinct aspects, namely the inhomogeneous character of local sensitivity on the surface of a nanoresonator, and the power of dual-wavelength surface plasmon resonance sensing (SPR) to provide more information with higher accuracy on the determination of important and parameters in the biomolecular detection of lipid vesicles with emphasis on the complex and biologically relevant exosomes.

Ch. 6 provides a basic description of stochastic diffusion-controlled reaction simulations, together with a summary of our results from *in silico* experiments.

Ch. 7 describes -omic approaches to profile and quantify the content of cells and extracellular vesicles in order to tease out commonalities and differences across cellular types and growth conditions.

Ch. 8 provides a short summary of the results in the appended papers.

Finally, future outlook and perspectives are offered in Ch. 9.

Chapter 2
Glioblastoma cells and extracellular vesicles

2.1 Glioblastoma

Gliomas originate from glial cells and are the most common type of malignant brain tumors [12]. The most common type of glioma is in turn astrocytoma. Glioblastomas (GBM) are a high grade aggressive type of glioma, constitute 15% of all brain tumors and 60-75% of astrocytomas [13].

A GBM cell population, as that of many tumors is highly heterogeneous and comprises also the presence of cancer stem cells (CSCs). These cells constitute the self-renewal and proliferative potential of a tumor owing to their stem-like characteristics. Various hypothesis exist on their origin including the evolutionary theory of cancer [14]. The first finding of CSCs in gliomas was accompanied by observation that the stem-like properties of tumor cells may be epigenetically induced and that a defective response to stimuli may contribute to the pathology [15]. However, the exact causes of gliomas and GBM initiation are unknown.

2.2 Primary cells vs. cell lines

In our work we include two commercially available glioma cell lines and two newly isolated patient-derived cell lines.

The commercial cell lines are HTB-14™ a.k.a. U-87-MG (I will refer to it as U87 in the following pages) and HTB-148™ a.k.a. H4, both purchased from ATCC®. U87 is considered a high-grade glioma and has been widely used in cancer studies. H4 is considered a low-grade neuroglioma and it is categorized as non-tumorigenic based on xenograft tests. It is hence seldom utilized in cancer research. The primary cells are CSCs recently derived from adult GBM patients [16].

Besides having been derived in different ways, the cells used in our studies, by their own nature, also differ in the culture conditions being used. In fact, U87 and H4 cell lines are typically cultured in the presence of fetal bovine serum (FBS), while CSCs are grown in defined serum-free medium [17]. Advantages of commercial cell lines over primary cells include their availability, robust protocols and characterization data, and in principle, their use as reference model systems for reproducible investigations. However, a recent DNA analysis revealed that long-term passaged glioma cell lines differ genetically from the original tumor leading to characteristics that may spoil some of the conclusions from research findings over the years [18].

2.3 Extracellular vesicles

Extracellular vesicles (EVs) are produced virtually by all cells and have an emerging role in understanding cellular communication. They are made of a double lipid bilayer and carry surface markers and a cargo rich in proteins and nucleic acids. EVs are secreted in the extracellular matrix and are found in all body fluids, such that they elicited hopes to develop novel diagnostic and prognostic targets. The complexity and heterogeneity of these tiny biological material is overwhelming. On one hand biomedical scientists are trying to assess

their origin, biological functionality, absorption and potency, while on the other their precise composition and quantification remain elusive.

With paper III we offer a review into the worlds of standard and state-of-the-art techniques that are used or are emerging as important tools to physically characterize and quantify extracellular vesicles in general and exosomes in particular. The introduction and references therein provide a background in the discovery, categorization, biogenesis, composition and function of extracellular vesicles and exosomes.

Chapter 3
Cellular stress

3.1 GBM, stress and extracellular vesicles

When solid tumors grow they usually create a dense mass of cancer cells void of blood vessels, which creates a hypoxic core, i.e. a region hence with less access to nutrients and oxygen. During radiotherapy on the other hand free radical species are formed, which lead to cell damage and ultimately cell death via oxidative stress pathways. Both types of stressors, hypoxia and oxidative stress lead to cellular responses with significant changes in gene expression and cell physiology.

Several studies have characterized exosomes from tumor cells of various origin[19], [20], how these vesicles are involved in cellular communication and pathology progression, how their protein and genetic content changes in response to a stimuli and how their differential composition upon stress impacts the effect on host cells in vitro or in vivo.

Exosomes isolated from murine brain tumors revealed their immunological role beyond the blood brain barrier [21]. EVs from the U87 cell line have been characterized in the context of hypoxic stress and their role in angiogenesis in particular and tumor progression in general has been documented. Angiogenic tests, which model particular aspects of blood vessel formation, with U87-derived and other cancer-derived EVs are normally conducted in vitro using human umbilical vein endothelial cells (HUVECs) as a model system. Based on tube formation or migration capacity of these endothelial cells, exosomes from U87 under hypoxia were shown to contain elevated levels of angiogenic proteins and mRNAs [22]–[24], which identified extracellular vesicles released by cancer cells under hypoxia as mediator of tumor-induced angiogenesis. The effects of ionizing radiation on the protein composition of EVs has also been reported for head and neck squamous cell carcinoma [25] and in breast cancer cells that show hypoxia-induced resistance to treatment [26]. Moreover, cells in hypoxic cores are found to be therapy resistant. Hence hypoxia related extracellular signaling mediated by exosomes is likely to persist after radiation induced damage.

3.2 Hypoxia

When oxygen levels decrease in a cell the hypoxia inducible factor 1 alpha (HIF1a) [27], [28] accumulates and translocates to the nucleus where it binds to HIF1b and activates the transcriptions of several genes involved in general cell adaptation, such as stress response, energy metabolism, and a specific hypoxia response, such as the expression and release of angiogenic proteins.

Normal atmospheric oxygen levels present in cell culture systems correspond to around 18%, which is very high compared to tissue O_2 concentration in vivo. In the brain this level is even lower estimated at around 2-3% [29]. However, cells are adapted and considered to be in their normal growth conditions when cultured in standard incubators at 37˚C, 80% humidity, 5% CO_2 and 18-20% O_2.

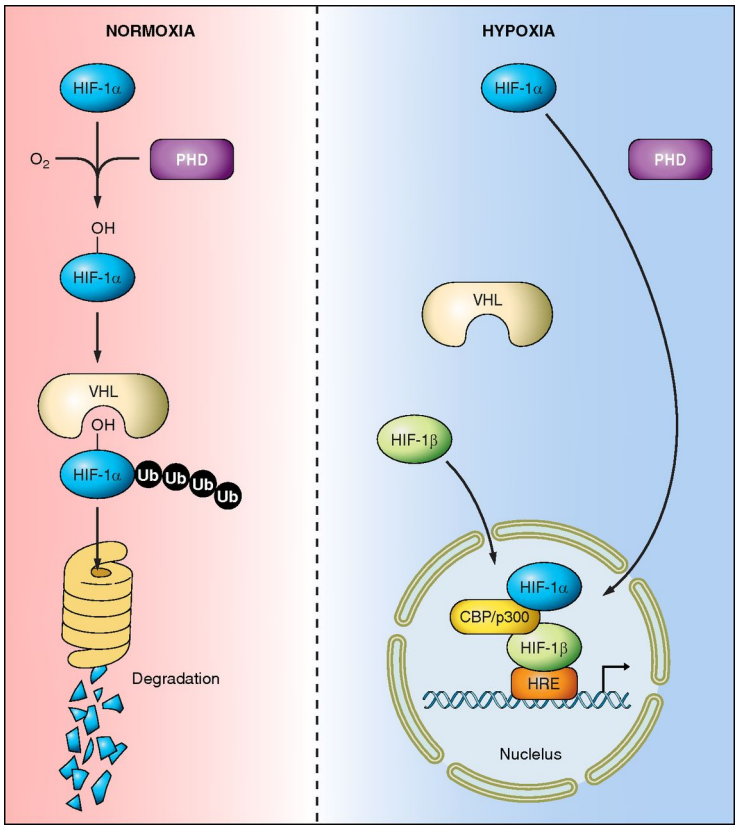

Figure 1 Schematic diagram illustrating the regulation of HIF-1α. Under normoxic conditions, prolyl hydroxylase domain (PHD) proteins use molecular oxygen as a substrate to hydroxylate HIF-1α. Once hydroxylated, HIF-1α binds the von Hippel-Lindau (VHL) protein and becomes polyubiquitylated (Ub) and targeted for proteosomal degradation. Under hypoxic conditions, PHD activity is reduced and HIF-1α escapes hydroxylation, accumulates and translocates to the nucleus where it binds with HIF-1β and CBP/p300 at the hypoxia response element (HRE). Reproduction from [30]

3.2.1 Experimental conditions

Hypoxic conditions in vitro are obtained using special incubators, which allow to flush nitrogen until a desired O_2 concentration is reached, while keeping CO_2 levels stable. Since the hydroxylation of HIF1a is both oxygen and iron dependent, hypoxia can be mimicked chemically by the administration of an iron chelator, which inhibits the function of PHD hence it leads to the accumulation of HIF1a.

H4 and U87 cell lines were seeded, low sub-confluency was reached after 48h, at which point they received fresh culture medium for the beginning of the experiment and were placed in a hypoxia incubator at 1% O_2 and 5% CO_2 at 37ºC for 4 and 24 hours. In a separate experiment, hypoxia was mimicked by the administration of different concentrations of DIP – an iron chelator commonly used as a proxy for hypoxia – at the 48h medium change. In this case cells were collected at 0.5, 1, 2, 4, 8, 24 hours.

3.2.2 ELISA detection of HIF1α

We tested the induction of hypoxic conditions by assessment of the level of HIF1a with an ELISA kit (Human/Mouse Total HIF-1α; R&D Systems, Inc., Minneapolis, MN, USA). U87 and H4 were seeded, after 48 hours standard medium or with the addition of various

concentrations of DIP was exchanged and cells were collected at several time points. In a later experiment, we tested the accumulation of HIF1a in a hypoxic chamber with 1% O_2.

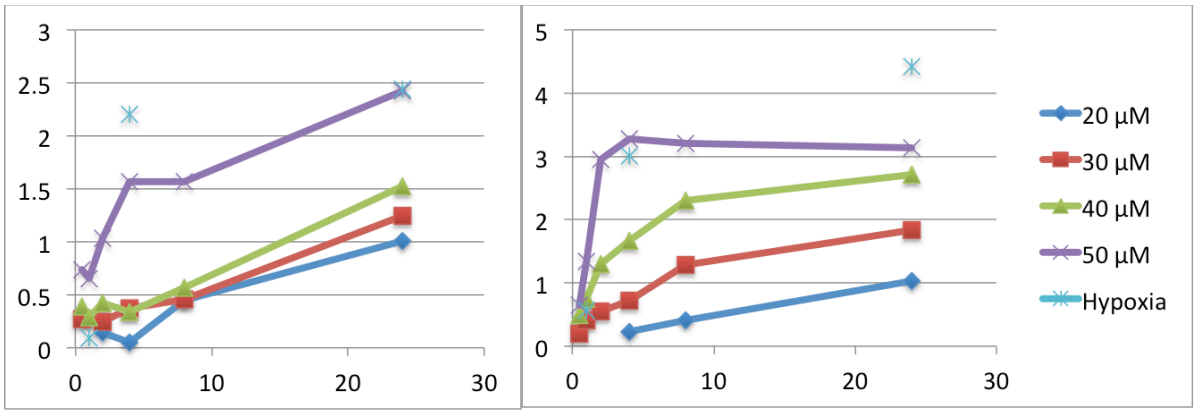

Figure 2 HIF1a ELISA after 0.5, 1, 2, 4, 8, and 24 hrs after administration of different concentrations of DIP or after 24 hrs of incubation in the hypoxia chamber, from cellular extracts from U87 (left) and H4 (right) cells. The y-axis represents the ratio of HIF1a in the treated vs. a single untreated at 24hrs.

Our results (Fig. 2) confirm DIP as a potent inducer of HIF1a. H4 cells are more sensitive to DIP than the U87 cells. Both cell lines respond strongly in few hours from treatment and start dying at higher doses (not shown). Hypoxia treatment with actual oxygen deprivation induces similar levels of HIF1a as the highest non-lethal dose of DIP.

3.3 Oxidative stress

Oxidative stress may have various causes but primarily manifests itself with the accumulation of reactive oxygen species and free radicals which lead to DNA damage, protein adducts and lipid peroxidation[31], [32]. Ionizing radiation recapitulates many aspects of oxidative stress [25]. Hence, oxidative stress models are relevant in the study of cancer.

As mentioned, one result of oxidative stress is the process lipid peroxidation that consists the degradation of lipids in the plasma membrane and other organelles. One byproduct of the degradation of arachidonic acid is a type of prostaglandin called 8-iso-PGF2alpha (PGF2a for shorts in this thesis) and it is used as a marker of non-canonical (non-enzymatic) lipid peroxidation induced by oxidative stress [33], [34].

3.3.1 Experimental conditions

All cell lines were seeded at an appropriate cell density in order to obtain low sub-confluency cultures after 48h, at which point they received fresh culture medium in order to begin the experiment. Oxidative stress was elicited by administration of tert-Butyl hydroperoxide (tBHP) [35] in a concentration of 20 µM for BAC-D0 cells, 30 µM for BAC-E3 and H4 cells, 50 µM for U87 cells. The concentration was chosen in such a way to minimize cell death (less than 20%) in order to avoid overabundance of debris in the supernatant. The cells growing in control or oxidative stress condition were placed back in the incubator and collected at different time points.

3.3.2 ELISA detection of PGF 2α

Post-culture U87-MG and H4 cells, including medium for controls and oxidative stress are hydrolyzed with 10N NaOH, for 2hrs at 45°C (1:1 dilution for cells and 4:1 for medium). Neutralization of samples is done with 12,1N HCL (pH adjusted to 6-8). The rabbit polyclonal anti-8-iso-$PGF_{2\alpha}$ in the kit is used for competitive binding of cellular 8-iso-$PGF_{2\alpha}$ or 8-iso-$PGF_{2\alpha}$ with an alkaline phosphatase (ALP) molecule covalently attached to it. After incubation at room temperature for 2hrs in a clear plate coated with goat anti-rabbit polyclonal antibody, the wells are washed and ALP made to react with its substrate, p-nitrophenyl phosphate (pNpp) for 45mins. The reaction is stopped with tri-sodium water and read immediately in a spectrophotometer at a wavelength 405nm. The lower is the signal, the higher the concentration of cellular 8-iso-$PGF_{2\alpha}$.

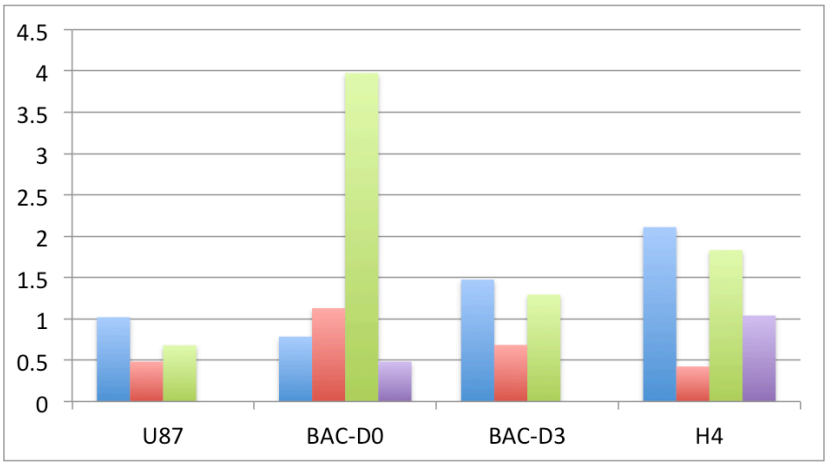

Figure 3 PGF2a ELISA in cellular extracts of U87, BAC-D0, BAC-D3 and H4, after 24 hrs administration of tBHP. The y-axis represents the ratio of treated vs. untreated. The colors represent separate experiments.

In our measurements we did not see a consistent increase of PGF2a in the treated vs. untreated samples, neither in cellular extracts (Fig. 3) nor in the supernatant from these cells (not shown). One major issue encountered in this test was the difficulty to account for volume changes during samples preparation. Moreover, we cannot be sure whether isoprostanes are retained in the cells, or if they accumulate in the medium, and if so, how fast they degrade. Overall we conclude that the concentration of PGF2a in our samples was not consistently above the limit of detection of the ELISA kit.

Chapter 4
Biosensing

4.1 Biosensors

A biosensor is a tool that detects the presence, and possibly also the amount of a biologically relevant substance, here referred to as the analyte. It does so by utilizing biochemical elements to interact with the analyte, and by transducing, that is by converting the information accessible by such interaction into a practically measurable (usually electronically) physical quantity that is the sensitive property of the sensor. This quantity can be, for instance, the force exerted on a micro-cantilever [36] upon contact with a micro or nano-scale object, or the change in the electrical conductance of nanowires [37], [38] due to changes in the environment, e.g. the introduction of a gaseous substance or the attachment of molecules. In general, one prefers label-free techniques, i.e. methods that can detect the analyte in its native state without the need to introduce e.g. a fluorescent label on the target. Each sensor type offers advantages and disadvantages and may be more or less suitable for a specific application. Light provides several transduction mechanisms as made evident by a great variety of optical biosensor techniques [39]–[43].

4.2 Surface-based biomolecular sensing

In this thesis focus was put on surface-based biomolecular sensors, in which the biomolecular interaction happens on a fixed surface properly designed to provide the physical mean of transduction and the biochemical elements required to attract the analyte of interest. In real samples, i.e. complex mixtures such as blood, one must normally also suppress nonspecific binding of interfering molecular species. Surface-based sensors are often label-free which makes them simple assay platforms and it gives the opportunity to access raw information on e.g. the kinetics of the receptor-analyte interaction.

Most of the concepts illustrated in this work are of general validity for all nanosensors, as will be explained later. However, specific examples from the area of plasmonic sensing will be used, since this work originated from the effort of optimizing plasmonic phenomena for sensing and bioanalytical applications.

4.2.1 Reaction vs. diffusion-limited regime

In a surface-based biosensor the sensitive surface is typically exposed to a liquid volume containing the analyte (label-free sensing). The final outcome of such biomolecular reactions is represented by the surface coverage, i.e. the amount of analyte bound to a given area of the sensor's surface. The amount of analyte bound after a certain time depends on the initial concentration of the analyte in the solution and on the kinetic parameters characterizing the reaction between the analyte and its receptor molecules in a manner typically described by the Langmuir isotherm:

$$\frac{d\Gamma}{dt} = k_{on} c_0 \left(\Gamma_{max} - \Gamma(t)\right) - k_{off}\Gamma(t) \qquad (1)$$

Here $\Gamma(t)$ is the time-dependent surface coverage, Γ_{max} is the maximum surface coverage achievable on the sensor, k_{on} the binding rate constant ($M^{-1}s^{-1}$) and k_{off} the unbinding rate constant (s^{-1}). The concentration at the surface is c_0 (the unit used for concentration defines the unit for Γ). When there are as many molecules leaving the sensor as there are attaching to it on average, an equilibrium condition is achieved and the equilibrium surface coverage Γ_{eq} can be estimated by setting the temporal derivatives to zero:

$$\Gamma_{eq} = \frac{\Gamma_{max}}{K_D/c_0 + 1} \qquad (2)$$

where $K_D = k_{off} / k_{on}$ is the dissociation constant.

The previous description (eq. 1 and 2) is valid in the so-called *reaction limited regime*, an approximation in which diffusion does not play a role in determining the local concentration of molecules at the surface available for binding. This is normally the case when the number of analyte molecules close to the sensor is relatively high compared to the number of available receptors. Usually this approximation is only valid after a certain waiting time, since initially, when all receptors are free, a depletion zone – a local volume near the surface with no or much less molecules than in bulk – is created as a consequence of the initial binding.

On the other hand, when concentrations are very low compared to the receptors' availability, and when the affinity is high, the surface coverage can become *diffusion* or *mass-transport limited*. Diffusion is macroscopically described by Fick's first and second laws:

$$\boldsymbol{J} = -D\,\nabla C \qquad (3-a)$$

$$\frac{\partial C}{\partial t} = D\,\nabla^2 C \qquad (3-b)$$

D is the diffusion constant, C is the concentration of the diffusing species, $\boldsymbol{J}$ is the flux density and it is generally a function of space and time.

The time-dependent surface coverage for an infinite planar surface in contact with an infinite liquid with bulk concentration c is found by solving Fick's equations with the proper boundary conditions [44]. The solution is given by:

$$\Gamma(t) = 2c\sqrt{\frac{Dt}{\pi}} \qquad (4)$$

Eq. 4 tells us that for infinitely high affinity (k_{off} = 0), after a long enough time all the receptors will be occupied. In practice, the temporal evolution and the equilibrium value of the surface coverage depend on the interplay between diffusion and reaction.

The system can then be modeled by coupling the Langmuir isotherm (Eq. 1) with Fick's second law (Eq. 3-b). There is no analytical solution to this problem. Finite element methods can be used to obtain both a steady state and a time-dependent solution. The dimensionless Dahmköhler number has been suggested as a means to determine whether a system exhibits mass transport or reaction limited binding kinetics [45].

4.2.2 Geometrical aspects of diffusion

It is important to notice that the full diffusion problem includes a 3D spatial dependence of the concentration. The spatial dependence disappears on the sensor surface when calculating

the surface coverage for symmetric situations such as the case of a planar surface, spherical sensor in a volume or hemispherical sensor on a flat substrate. Other than these cases, the presence of molecules on the sensor's surface presents a non-uniform distribution that depends on the geometry of the sensor itself.

This can be intuitively understood by considering a comparison between a hemispherical sensor and a disk-like sensor, placed on a flat substrate (Figure 1). Let us recall Fick's first law (eq. 3 a) and assume C to be finite far away from the sensor and $C=0$ at the sensor surface. For the sake of clarity, in this example let us assume that the sensor is a perfect absorber and at all times $C=0$ at its surface. Let the molecules diffuse. The angular distribution of the flux around the hemisphere will be uniform due to symmetry and the probability to capture a molecule is equal for any point of the hemispherical surface. Now imagine squeezing the hemisphere against the substrate, making it more disk-like. What happens to the flux lines? The concentration and its gradient for this geometry are not uniform over the sensor surface due to a loss of symmetry. Therefore the flux lines will "adjust" to the new gradient by becoming denser at the edges than at the center of the flattened hemisphere. Consequently, the probability of capturing molecules is not uniform over the surface of a disk, and becomes higher the closer you are to the circumference.

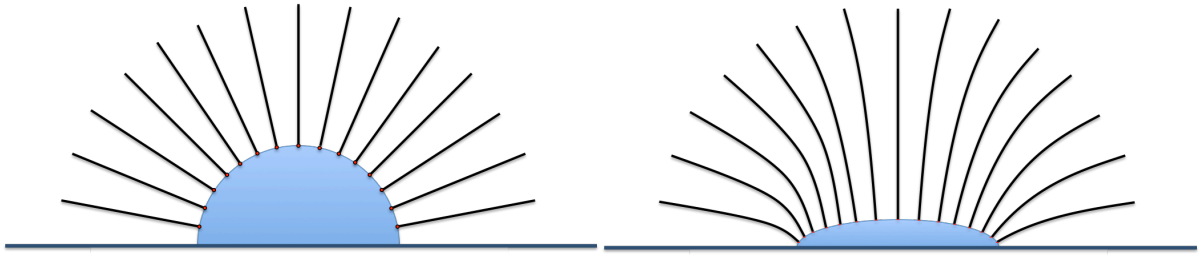

Figure 4 Illustration of the diffusion flux lines for a hemispherical absorber (left) and a flat disk-like absorber (right). The flux lines are homogeneous for the hemisphere, and inhomogeneous for the disk geometry.

Fig. 4 illustrates the former example. The analytical solution for the steady-state flux to a completely flat disk is given by [46]:

$$j(r) = \frac{2DN_A c_0}{\pi\sqrt{a^2 - r^2}} \quad , \quad r < a \qquad (5)$$

where N_A is the Avogadro number, c_0 is the initial solution concentration (assumed to be constant everywhere in the solution) and a is the radius of the disk. From Eq. 5 it can be seen how the flux is significantly higher as r approaches the edge.

For more complex structures it can be said that usually corners and edges will be exposed to denser flux lines than concave regions of the sensor or convex surfaces with small curvature. The geometry dependence of capturing probability is discussed in Paper II, where we look at the site-dependent binding probability obtained for various sensor shapes from stochastic simulations.

4.3 Estimating vs. counting

As the sensitivity and limit of detection are constantly being improved, incredibly small concentrations in the sub-picomolar range are being detected [47]–[50]. To give an idea, 1 fM corresponds to approximately 600 molecules per cubic millimeter, while a nanosensor with a

diameter of 100 nm (10000 times smaller than 1 mm) can be covered by about 300 receptor molecules. To put it bluntly, this means that for small sensors the number of molecules in a thin layer in the vicinity of the receptors is zero at almost all times, although the concentration is finite, and some of the time it is 1 or at the most 2. Under these conditions the concept of concentration itself breaks down and the equations for a continuous model illustrated above loose the validity and accuracy that they provide in macroscopic descriptions. They can only provide an average description of a system, but each individual experiment will likely deviate strongly from this result simply by chance.

To understand the fluctuations in the system due to the individual molecules, one must adopt stochastic descriptions and numerical simulations of stochastic events instead of continuum models. Diffusion is easily modeled by discretizing either time or space, and calculating respectively either diffusive jumps or time intervals between jumps of pre-determined length, according to probabilities which accurately describe diffusion processes. The incorporation of chemical interactions into such models is more challenging, mainly due to the problematic translation of the reaction constants into temporal and spatial parameters at the single molecule level. At this scale, in fact, a description based on molecular dynamics and energy potentials would be appropriate, but computationally and theoretically very demanding. However, several algorithms exist to simulate stochastic diffusion-reaction processes. In Chapter 5 we will briefly describe some basic aspects of this type of simulations and the implementation for our single-molecule noise study.

4.4 End-point vs. real-time detection

Current commercially available sensing tools are based on ensemble averaging over either large (active spot size of several mm) uniform areas – such as SPR [51] and quartz crystal microbalance (QCM) [52] – or large collections of sensing nanoentities [53], [54]. The sensing schemes can then be categorized into end-point and real-time detection. In an end-point assay, such as the enzyme linked immunosorbent assay (ELISA) [55], after a certain number of reactions have taken place in order to capture the analyte onto the sensor's surface, the only information accessible is the final surface coverage, which can be related to the original concentration in solution upon prior calibration of the device. In fact, even quantifying the surface coverage can be difficult and ELISA tests are normally used for yes/no diagnostic tests.

In contrast, for real-time assays, the reaction utilized to bind the analyte is followed over time, until equilibrium is reached. Again, thanks to prior calibration, the signal produced by the equilibrium surface coverage is an indication of the concentration. However, the curve can also be fitted in order to extract reaction rate constants (k_{on} and k_{off}). It is also easier to verify that the system has actually reached equilibrium by looking at the binding curve.

Increasingly faster and less noisy detectors represent an improvement in this direction. Higher acquisition speed and signal-to-noise ratio (SNR) allow performing fluctuation analysis [56], [57] by relying on the finer details of the signal. The latter approach was shown to provide more accurate estimation of the reaction rates than conventional curve fitting.

4.5 Single-molecule sensing vs. complex ensemble of nanoparticles

As we have seen, considerable improvements in sensitivity and temporal resolution have led to the real-time detection of single-molecule events in some systems. On one hand ensemble average offers high accuracy due to the large number of events detected, on the other hand single molecule counting provides access to the understanding of molecular properties and interactions. For instance, it offers the possibility to determine reaction parameters in situations where few units of a certain biochemical species are present in clinical samples, as well as having the potential to discriminate between the competing reaction species binding to the same receptor(s). As D. R. Walt puts it, "counting molecules is as good as it gets" and optical detection methods have proven to provide the most accurate and less invasive tools for achieving this goal [6].

For example Mayer *et al.* [57] showed single-particle LSPR detection of single-molecule binding and unbinding events by analyzing sensitive signal fluctuations. Chen *et al.* [50] utilized amplified detection in a multiplexed end-point scheme and Poissonian fitting to relate the signal, produced by few molecular binding events to plasmonic nanosensors, to the concentration in solution. More recently, scientists have achieved single-particle single-molecule sensitivity in real-time [58]–[61]. This is believed to be the ultimate sensing platform, albeit the present technological limits of reproducibility, parallelization, and cost.

In the next section we discuss the need to gain deeper understanding in the origins of signal variation in situations when few molecules are being detected.

Despite the advances of single-molecule sensing, certain fields need still to rely on ensemble measurements. The heterogeneity and biochemical complexity of extracellular vesicles makes them on one hand ideal candidates for interesting single-vesicle experiments, on the other it poses great limitations to the progress on their investigation. In fact, since physical sensing depends on several physical parameters that relate to the biomolecular nature, shape and size of vesicles [62], ensemble measurements are very important to assess a range for the determination of the concentration, an estimate deviation from the mean and its root causes. This type of problem is addressed further in section 2 of Ch.5 where we also discuss how careful ensemble measurements and theoretical modeling enabled the characterization of a sub-population of exosomes.

4.6 Noise and uncertainty issues

When measuring low signals or small changes in a signal, it is necessary to keep in mind what can affect the signal-to-noise ratio (SNR) of the measurement at the intensity being measured. Photodetectors are subject to several types of noise, briefly listed hereafter: dark noise, i.e. generation of thermal electrons (it can be reduced by cooling); read-out noise when measuring the charge of a pixel (it can be practically eliminated by amplification); background noise due to photons collected from other sources than the sample (it is convenient to measure in the dark); shot noise, stemming from the discrete nature of the measured signal (photon or electron flux). In contrast to the other noise sources, shot noise is not possible to eliminate and it increases proportionally to the signal. In fact, it follows Poissonian statistics, hence the fluctuations in the signal are proportional to $\sqrt{N}$, where N is the number of photons or electrons being detected.

This means that as the absolute signal level (N) increases, the relative contribution of all other noise sources is reduced and the noise is mainly due to shot noise. However, the change in intensity one aims to measure in the sensing experiment is normally proportional to N. For instance, a plasmonic nanoparticle could change its light scattering yield by 0.01% when a molecule attaches to it. Therefore, SNR ~ $N/\sqrt{N} \sim \sqrt{N}$ and the influence from shot noise is reduced at higher intensities. In other words, although the noise level in N increases, the change in N increases more. On the other hand, when N is small, all noise sources matter and should be minimized. This includes also minimizing sources of signal instability, such as mechanical vibrations and thermal fluctuations. Moreover, in plasmonic sensing, accurate determination of the resonance wavelength requires careful data analysis [63], ranging from curve fitting to centroid determination, rather than simple observation of the maximum position of a noisy peak.

It is possible to achieve shot noise-limited measurements when measuring on large areas [64] but practically impossible when measuring on single nanosensors due to the limited number of photons/electrons. Assuming one can exploit such an optimum system and apply the best data analysis techniques [65], a level of uncertainty remains in the quantitative characterization of signal changes originating from biomolecular interactions occurring at the sensor's surface. Unless all molecular binding events are clearly observed one by one, translating e.g. the plasmonic spectrum change into number of molecules bound can be very challenging.

First of all, the signal change produced by a molecule binding to a nanoresonator is not constant for all binding events. In addition to being dependent on the size of the molecule, it also depends on where on the nanosensor the molecule binds. In fact, most nanosensors show a spatial dependent sensitivity distribution [66]–[69], which leads to varying signal amplitudes, and an uncertainty [70] in quantifying the source of the signal change, *e.g.* surface coverage or exact number of molecules binding/unbinding. Moreover, in the few molecules limit, the poor statistics compared to the experimental noise add to the complicacy of making good use of the data.

The local sensitivity of plasmonic resonators will be addressed in Ch. 5.5 and it is dealt with in detail in Paper I. In Paper II we consider such inhomogeneous sensitivity in conjunction with the influence of sensor geometry on the preferential binding locations and we discuss the implications for signal accuracy in ensemble measurements and clear observation of single-molecule binding/unbinding events.

Chapter 5
Plasmon resonances

5.1 Surface plasmon resonance (SPR)

It is a known fact that the reason why metals are good conductors is because the outermost electrons in metal atoms are not bound; hence, electromagnetic fields can induce electron movement in an orderly fashion, generally referred to as current. These electrons are said to constitute a free-electron gas. At the interface between a dielectric and a conductor, they can interact with electromagnetic field oscillations, giving rise to collective excitations called surface plasmon polaritons (SPPs).

The surface plasmon resonance (SPR) effect can be described in terms of the dispersion relation of the surface plasmons (Eq. 6). By solving Maxwell's equations with the proper boundary conditions for two semi-infinite materials (metal and dielectric) [71], we find the plasmon wave vector:

$$k_{SPP}(\omega) = \frac{\omega}{c_0}\sqrt{\frac{\varepsilon_m(\omega)\varepsilon_d}{\varepsilon_m(\omega)+\varepsilon_d}} \qquad (6)$$

where the dielectric response is characterized by the dielectric constant $\varepsilon_d = n_d^2$, n_d is the refractive index and the metal properties are described by the complex dielectric function ε_m. To a first approximation the energy dependence of ε_m can be described by the Drude model [72]. However, this does not reproduce experimental data accurately at all frequencies, e.g. damping at high frequencies (blue light) in the case of gold. A better model is found by the introduction of a damping in the equation of motion of the electron, leading to a Lorentzian solution for ε_m. For sensing purposes, the most important message from Equation 6 is that the wave vector k_{SPP} is greater than the light line in the adjacent dielectric medium when this is air (n = 1) or water (n = 1.33). Therefore, due to the requirement of conservation of momentum, the surface plasmons cannot be excited by simply shining light on a metal surface.

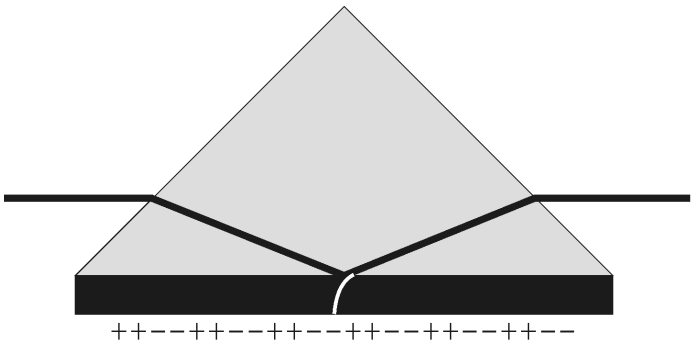

Figure 1 Representation of Kretschmann configuration for SPPs excitation. The light passes through a prism and hits the metal film at a high incident angle. The evanescent field is coupled into SPPs at the metal/environment interface. (Courtesy of T. Antosiewicz)

One possibility to achieve SPR is to use a higher refractive index medium (hence higher wave number) on the opposite side of a finite film to couple light into a plasmon running at a gold/water interface. The SPR is then observed as a minimum in the reflected light signal.

This is achieved through the use of a glass prism (n = 1.5) and it is known as Kretschmann geometry [73], arguably the most common configuration for SPR based sensing (Figure 2). The changes in SPR signal can be related to changes in refractive index [74] and give relatively accurate quantitative information on analyte coverage due to the planar surface geometry (1D spatial sensitivity distribution).

Surface plasmons are waves characterized by a propagation length along the interface and a decay length (or penetration depth) into the medium. The shorter the decay length of the exponentially decaying transverse field, the better he confinement is said to be. However, the propagation length is reduced (higher imaginary wave vector) since the field becomes more focused to the lossy metal (for an understanding of SPPs mode confinement the reader may refer to [71]). In terms of sensing, this means that what happens far (~100 nm) from the gold/water interface – a change in the refractive index in the bulk medium – produces a smaller effect on the SPR spectral position and line-shape, than the same change happening at the surface.

5.2 SPR shift

The shift in wavelength or angle of the SPR minimum in the intensity of reflected light due to a change in the refractive index of the medium in contact with the metal surface supporting the surface plasmons is referred to as the SPR response, R. For a film thickness d_f and refractive index n_f in contact with a bulk medium of index n_b, R can be expressed as[74]:

$$R = S(n_f - n_b)[1 - \exp\left(-\frac{d_f}{\delta}\right)] \quad (7)$$

where δ is the decay length of the SPR evanescent field intensity and S is the sensitivity, usually expressed in SPR signal per change of bulk refractive index units.

One can introduce a dimensionless factor φ to take into account the relationship between δ and d:

$$\varphi\left(\frac{d_f}{\delta}\right) = [1 - \exp\left(-\frac{d_f}{\delta}\right)]\frac{\delta}{d_f} \quad (8)$$

hence φ is close to unity for thin films of thickness $d_f << \delta$.

We can introduce the quantities v_m as the integral volume of molecules forming a nanoparticle, c_* as the concentration of molecules per unit volume. Additionally, if a film is made of a supported layer of nanoparticles, we call c the surface concentration of nanoparticles. It can be shown that:

$$c_* = \frac{\Delta\Gamma_f}{d_f} = \frac{n_f - n_b}{\frac{dn}{dC_*}} \quad (9)$$

where $\Delta\Gamma_f$ is commonly referred to as surface coverage and is equal to $c_* d_f$, i.e. the number of molecules in a film per unit surface area, or $c\, c_* v_m$ for a film made of nanoparticles, and dn/dC_* is the derivative of the refractive index with respect to the bulk molecule concentration. The SPR shift in eq. 7 can be rewritten in a more general form:

$$R = S\frac{dn}{dC_*}cc_*v_m\frac{\varphi}{\delta} \quad (10)$$

By rewriting the volume term in eq. 10 for the appropriate geometrical case (e.g. a film, a layer of spherical beads, or a layer of deformed or non-deformed vesicles) one can obtain an expression for the dimensionless factor φ. In particular, for a layer of undeformed vesicles of radius r :

$$\varphi\left(\frac{r}{\delta}\right) = [1 - \exp\left(-\frac{2r}{\delta}\right)]\frac{\delta}{2r} \quad (11)$$

which can be replaced by eq. 8 provided that the film thickness d_f is simply written as the general layer thickness $d=2r$. As long as $r < \delta$, this expression for φ is nearly identical for spherical beads and undeformed vesicles.

5.2.1 Dual wavelength SPR

The simultaneous measurement of SPR shift at two different wavelengths allows for the simultaneous and more precise determination of both the size and – if binding is diffusion limited – the bulk concentration of nanoparticles. This section describes the physical basis for extracting this information.

Various terms in the expression for the SPR shift for a homogeneous film, a layer of beads or vesicles, represent wavelength-dependent physical parameters, namely S, dn/dC_*, δ and $\varphi(d)$ for any d/δ ratio. From eq. 10 it follows that:

$$\frac{R_{\lambda_1}}{R_{\lambda_2}} = \frac{S_{\lambda_1}}{S_{\lambda_2}}\frac{(dn/dC_*)_{\lambda_1}}{(dn/dC_*)_{\lambda_2}}\frac{\varphi_{\lambda_1}}{\varphi_{\lambda_2}}\frac{\delta_{\lambda_2}}{\delta_{\lambda_1}} \quad (12)$$

Size determination

Therefore, if one knows the values of S, dn/dC_*, δ at two wavelengths λ_1 , λ_2 and the specific dependence of $\varphi(d)$, by measuring the change of SPR signal at these two wavelengths, the thickness d of the layer that produced these shifts (or $2r$ for a layer of particles of radius r) can be determined by the ratio $R_{\lambda_1}/R_{\lambda_2}$. For a thin film where $d << \delta$ eq. 12 further simplifies to:

$$\frac{R_{\lambda_1}}{R_{\lambda_2}} = \frac{S_{\lambda_1}}{S_{\lambda_2}}\frac{(dn/dC_*)_{\lambda_1}}{(dn/dC_*)_{\lambda_2}}\frac{\delta_{\lambda_2}}{\delta_{\lambda_1}} \quad (13)$$

Hence one can measure the sensitivity at two wavelengths, obtain literature values of the wavelength and concentration dependence of the refractive index for a given substance that forms a thin film on the SPR substrate, measure the SPR shifts' ratio upon thin film formation and use eq. 13 to calibrate a dual wavelength sensing experiment by finding the $\delta_{\lambda_2}/\delta_{\lambda_1}$ ratio.

Bulk concentration determination

Thereafter, in combination with eq. 12 and the specific form of φ (e.g. eq. 11) one can determine the radius of nanoparticles of size comparable to the decay length.

Under diffusion-limited steady-state flow conditions, Fick's equations 3-a,b solved with the boundary conditions for a rectangular channel yield the following solution [75] for the surface concentration:

$$c(t) = C\xi(D^2Q)^{1/3}t \quad (14)$$

where C is the bulk concentration of nanoparticles, D is the diffusion constant (inversely proportional to the particles size), ξ is a geometrical constant related to the geometry of the flow cell, and Q is the volumetric flow rate. By substituting eq. 14 in eq. 10 one can determine the bulk concentration:

$$C = \frac{R(t)}{A\xi(D^2Q)^{1/3}t} \quad (15)$$

with $A = S\frac{dn}{dc_*}c_* v_m \frac{\varphi}{\delta}$.

5.2.2 SPR measurements of exosomes

In addition to the accuracy issues described in Section 5.6, the determination of size and concentration of heterogeneous nanoparticles such as exosomes is subject to also other and more severe sources of uncertainty, some of which can be removed by complementary measures, including the advantageous dual-wavelength SPR sensing method.

Deformation of vesicles upon binding

Vesicles are non-rigid objects and can be subject to shape deformation upon binding. Rupert *et al.* [76] investigated this phenomenon in previous work and introduced a formalism to specifically account for vesicle deformation in the expression of φ and hence obtain a better estimate of the bulk concentration. However, in order to quantify the binding of particles of a size comparable to the SPR evanescent field decay length one must rely on knowledge of the thickness of the film forming on the substrate. The degree of deformation on the substrate cannot be deduced from the particle size in solution nor can it be determined with a single wavelength SPR measurement, but it can indeed, as described above, be estimated with high accuracy using dual-wavelength SPR sensing.

Heterogeneous sample

Artificial lipid vesicles and native exosomes can be dimensionally characterized by an average size, but a given sample displays a more or less broad size distribution. This aspect has also been addressed in previous work [76] by the introduction of an extended formalism to model the surface coverage of exosomes.

As described in Ch. 3, these vesicles, are also very complex in their composition such that their categorization in sub-populations based on surface markers has become an important aspect of their characterization. However, when targeting for measurement a specific sub-population in a complex exosomes samples, it can be that the mean physical characteristics of such population differ from the mean of the whole sample.

In Paper IV dual-wavelength SPR measurements and an extended formalism for the SPR response to films, rigid beads, and both deformed and undeformed vesicles were combined with complementary techniques (NTA, fluorescent NTA and TEM) to obtain, with high accuracy, information on the size determination of exosomes, the degree of deformation upon binding of CD63 positive exosomes, and an estimate of their bulk concentration as a sub-population of the total suspended exosomes that is better than what is attained with other methods so far used to quantify exosomes.

5.4 Localized surface plasmon resonance (LSPR)

Collective electron excitations can be observed also in small metal objects. When the size of the object is smaller than the resonant wavelength, the electric field of incoming light can polarize the whole particle "almost at once". In this case, we talk about localized surface plasmon resonance (LSPR) since the electrons, though free to oscillate, are not free to propagate beyond the particle's boundaries. The polarizability describes how a nanoparticle behaves in interaction with incoming electromagnetic energy. The polarizability for a spherical isotropic object can be derived in the quasi-static approximation and is given by:

$$\alpha(\omega) = 4\pi\varepsilon_0 r^3 \frac{\varepsilon_m(\omega) - \varepsilon_d}{\varepsilon_m(\omega) + 2\varepsilon_d} \qquad (16)$$

where r is the radius of the sphere, ε_d is the dielectric constant of the surrounding medium and ε_0 is the permittivity of free space. A resonance condition is obtained by setting to zero the denominator in Eq. 8, giving $\Re[\varepsilon_m(\omega)] = -2\varepsilon_d$.

For non-spherical objects the polarizability is a tensor and in general the resonant frequency of a metal nanoparticle depends on its material, volume, shape, and the refractive index of the surrounding medium. The polarization field of the nanoparticle adds to the electric field of the incoming light. At resonance the field generated by the particle is the strongest, so it is said that the field there is locally enhanced relative to the incident field. The field, in a first approximation, decays away from the particle like the near-field term of a dipole, i.e. $1/d^3$ where d is the distance from the resonator.

As previously mentioned for SPR sensing, the magnitude of the change in the response of a LSPR depends on the distance from the sensor. This can be expressed in terms of bulk sensitivity versus local sensitivity. Svedendahl *et al*. [77] compared experimentally the bulk and local sensitivity between SPR and LSPR refractometric sensing schemes. The study demonstrated comparable performance of LSPR and SPR in detecting local changes, e.g. molecular binding, thanks to the higher field confinement of metal nanostructures compared to the thin film counterpart, and despite the much higher bulk sensitivity of SPR. It is of practical importance to notice that for equal sensitivity one advantage of using nanoparticles rather than thin films is that light coupling is trivial and it does not require the use of a prism and bulky configuration. Both transmission and reflection measurements can easily be performed. Another advantage (at least for single molecule resolution) is that it is relatively simple to perform measurements on single nanoparticles, which represents a very miniaturized sensor. Chen *et al*. [50] demonstrated the capability of multiplexed end-point single particle dark-field spectroscopy in ELISA assay with ultra-sensitivity. Other recent works support the great potential of LSPR for single-molecule detection (see Ch. 4.5).

In the following section I will focus on the sensitivity of a plasmonic nanoresonator, pointing out how the local sensitivity is inhomogeneous in the vicinity of the sensor's surface.

5.5 Dipolar coupling and LSPR shift

The response to light of two objects in proximity of each other is not simply the superposition of the singular responses, but also the interaction between their individual responses should be taken into account. If their dimension is smaller than the wavelength of the incoming light, their response can be modeled by a dipole and their interaction can be considered in the

framework of the Couple Dipole Approximation (CDA) [78]. The electric dipole induced by light in one object, produces a polarization field that contributes to the total field which influences the neighboring object, and vice-versa. So the total induced dipole polarization for a molecule (1) and a metallic particle (2) can be written as:

$$\bar{P}_1 = \tilde{\alpha}_1\left(\bar{E}_0 - \tilde{A}_{12}\bar{P}_2\right) \qquad (17-\text{a})$$

$$\bar{P}_2 = \tilde{\alpha}_2\left(\bar{E}_0 - \tilde{A}_{21}\bar{P}_1\right) \qquad (17-\text{b})$$

where $\bar{E}_0$ is the incident field, $\tilde{\alpha}_1$ and $\tilde{\alpha}_2$ are the polarizability tensors of the two objects, and $\tilde{A}_{12} = \tilde{A}_{21} = \tilde{A}$ is the dipole mutual coupling term, which is also a tensor depending on the relative position of the objects with respect to each other and the direction and polarization of the incoming field. For the sake of simplicity we consider here only spherical objects and we drop the vector notation in Equation 17-a,b. The polarizability for a spherical object is given by eq. 7, which in air becomes:

$$\alpha_i = 4\pi\varepsilon_0 r_i^3 \frac{\varepsilon_i - 1}{\varepsilon_i + 2}, \quad i = 1,2 \qquad (18)$$

where r_i is the radius of sphere *i*, and the dielectric function ε_i is in units of ε_0.

By inserting P_1 (Eq. 17-a) in the expression for P_2 (Eq. 8-b) we obtain:

$$P_2 = \frac{\alpha_2(1 - \alpha_1 A)}{1 - \alpha_1\alpha_2 A^2} E_0 \qquad (19)$$

Equation 19 describes the response of the interacting system. By setting the denominator to zero we can calculate the mode frequencies. Moreover we can extract an expression for the effective permittivity ε_2 of the metal resonator with the molecule present:

$$\varepsilon_2(\omega_Q) = -\frac{2+Q}{1-Q} \qquad (20)$$

where $Q \triangleq (4\pi\varepsilon_2)^2 (r_1 r_2)^3 \frac{\varepsilon_1 - 1}{\varepsilon_1 + 2} A^2$ is a parameter that depends on the mutual coupling *A*, their radii and the permittivity of the dielectric ε_1.

For Q = 0 (no coupling) in Eq. 11, $\varepsilon_2(\omega_0) = -2$, which is the resonance condition obtained by minimizing the denominator of the polarizability of a single metal nanosphere (Eq. 7). It is possible to derive an expression for the relative resonance frequency shift $\overline{\Delta\omega}$ upon introducing a molecule near the particle. Without showing the derivation, in the case of small coupling (Q<<1), using Drude's dielectric function for ε_2 and considering that in the near field the coupling term A between a metal sphere and a molecule on its surface is proportional to $1/4\pi\varepsilon_0 r_2^3$, we can write the result:

$$\overline{\Delta\omega} \triangleq \frac{\omega_Q - \omega_0}{\omega_0} \sim -\frac{1}{2}\frac{V_1}{V_2}\frac{\varepsilon_1 - 1}{\varepsilon_1 + 2} f \qquad (21)$$

From this relation it is evident how the change in resonance frequency is proportional to the ratio between the volumes V_1 of the molecule and V_2 of the metal particle, on the polarizability of the analyte ε_1, and on a factor f (stemming from the coupling term *A*), which, to a first approximation, is proportional to the square of the local field enhancement.

For the purpose of this thesis it is important to remind the reader of the fact that the polarizability of the molecule results in a small though obviously non-negligible disturbance of the plasmon oscillations in the metal object. This means that the details of the molecule's polarizability may be disregarded in most cases, except for those instances where the aim is to understand intrinsic properties of the molecule in interaction with light, and the coupling of

the oscillation is strong, for instance in the presence of a nanoantenna with resonant frequency close to the energy involved in molecular state transitions. Instead, the polarizability of the metal particle is dependent on its size and shape, and, as we said, its orientation with respect to the incoming electromagnetic field. Hence, the coupling term Q is highly dependent on the molecule's position with respect to the resonator. An analytical expression exists for the polarizability of an ellipsoid. However, this is a tensor and it hampers the possibility to use the approach above to obtain meaningful expressions for the position-dependent resonance shift. For ellipsoids and more complex structures one has to recur to numerical methods. In Paper I we illustrate a method to calculate the resonance shifts based on the local field intensities of the different constituents of the interacting system and compare it to Finite Difference Time Domain (FDTD) simulations.

Chapter 6
Simulations of single molecules binding to single particles

6.1 Stochastic diffusion-controlled reactions

As anticipated in Chapter 4, for most purposes it is rather simple to simulate diffusion, and in the case of planar surfaces analytical expression can be obtained (see eqs. 4 and 14). However, the inclusion of reaction is a tricky business and it has been challenging biomathematicians for over a century.

Diffusion is a continuous process by which objects of various dimensions trace ballistic trajectories in the medium in which they find themselves [79]. At the macroscopic level, Fick's laws describe diffusion in terms of continuous changes of concentration, while at the microscopic scale the trajectories of single diffusing objects are described by discrete jumps constituting a "random walk".

Smoluchowski first developed a theory for diffusion-controlled reactions [80] later revised by Collins and Kimball [81]. Gillespie laid the foundation for the stochastic simulation algorithm (SSA) [82] . This model was later developed and expanded by many, as well as new models being established [83]–[87] resulting in an acceleration of the simulation time, but most importantly improved spatial resolution and temporal accuracy. One example of the application of stochastic diffusion-controlled reaction modeling is the study of dynamic compartmental models for the realistic description of biological systems and their kinetics [88].

In our simulations we model diffusion through a Wiener process [89] such that, given the diffusion constant *D*, the mean diffusion length in a time interval *dt* is equal to $s = \sqrt{2Ddt}$.

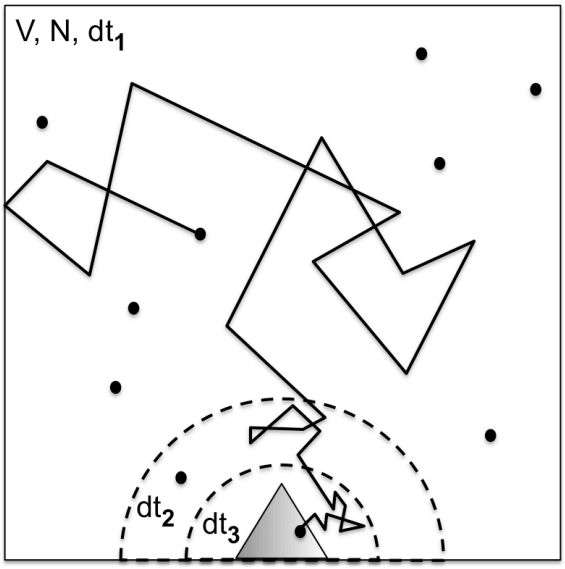

Figure 9 Schematic representation of the multi-time discretization stepping algorithm used in our simulation scheme. A box of volume V (side view) contains N molecules. The box has reflective boundaries. An absorber is located on one side (bottom). The molecules randomly diffuse at every time step dt. The time step has a different value in different regions, such that $dt_1 > dt_2 > dt_3$. As a consequence the diffusive jumps far from the absorber are on average bigger than in the hemispherical volumes closer to the sensor.

At each time step the spatial shift in *x*, *y*, and *z* directions is calculated by multiplying *s* by a random number drawn from the normal (0,1) distribution. So the mean diffusion step in all directions is equal to zero, while the mean absolute value and the standard deviation in 3D are both equal to $\sqrt{6Ddt}$ [90]. A cubic volume V, with a nanosensor located on one side of the cube, is filled with a fixed number of molecules N such that N/V is the desired concentration. By using multi-time discretization steps it is possible to simulate very small concentrations, while keeping a statistically significant N. This means that molecules far from the nanosensor explore bigger volumes than molecules close to the sensor in the same simulation time. Attention must be paid to the choice of the time steps, such that the molecules diffusing in proximity of the nanosensor undergo jumps that are on average much smaller (in our model <10X) than the characteristic size of the sensor. Figure 9 offers an illustration of the simulation scheme.

The sensor surface is discretized in fixed receptors locations. If any molecule is close to a binding receptor we evaluate the binding probability within the relevant time step, in this case dt_3 (see Figure 9Figure). Concurrently, in each time step the unbinding probability of already bound molecules is evaluated and if an unbinding attempt is successful, the molecule begins to diffuse from the next time step. The probability of binding P_b to any receptor is given by $P_b = 1 - \exp\left(-\sum_{receptors} r_c\, dt\right)$, where $r_c = k_{on}/V_r$, k_{on} being the binding rate, and V_r the spherical reaction volume of radius r_c given by the distance between the molecule and the receptor [82], which is non-zero only if the receptor is free. The sum runs over all receptors whose distance from the molecule is less than a critical distance.

Several sensor geometries and diffusion/reaction parameters are utilized. The model offers a platform for *in silico* single-molecule sensing experiments. In the following section the main results of Paper II are summarized, accompanied by future outlook on the use of the model hereby developed.

6.2 Results

The time evolution of binding/unbinding events on the sensor's surface can now be simulated with single event resolution.

The analysis of multiple such time-traces allowed us to track the position dependent binding probability for different sensor geometries. For instance, as it is expected, a receptor located on the tip of a cone will on average be occupied much more easily than at the base of such cone. This effect obviously fades away as a high equilibrium surface coverage is approached, due to modification of the sensor's landscape as seen by the molecules diffusing nearby as a consequence of receptor's occupation. However, the effect for low surface coverage (Γ< 15%) is non-negligible at equilibrium, as it can produce a difference in binding probability between two receptor locations of around 20%.

We also used the model to study the effect of LSPR inhomogeneous sensitivity distribution on the uncertainty of the signal produced by molecular binding and unbinding events. For instance, it was shown that the standard deviation of the signal is higher for a nanodisk under polarized than unpolarized illumination. It should be noted that this approach is not at all limited to plasmonic sensing, since the sensitivity maps of any type of sensor can be plugged in for analysis.

Chapter 7
Omics based characterization of EVs

7.1 Proteomics

The human genome contains approximately 20000 protein-coding genes [91]. Today the Uniprot Knowledgebase database for the human proteome contains over 70000 proteins including post-translational modifications [92], [93]. Proteins can be detected and studied in two principles ways: i) by immunodetection (i.e. using antibodies); ii) by mass-spectrometry.

The use of antibodies for protein detection and quantification has been arguably the most common method so far and has enabled e.g. molecular microscopy to flourish and many discoveries to be made. However, several limitations and problems may be encountered when trying an antibody for the first time, or the same antibody for a new type of sample or when looking at the reproducibility of results across experiments or biological materials or labs [94]. Until all actors undertake broad conjunct efforts to improve the standardization of antibodies production and use, researchers can safely rely only on extensive in-house validation and detailed reporting [95]. Despite these shortcomings, antibody detection of exosomes is very popular as it allows assessing an exosome sample's purity with respect to the cellular lysates by looking for an enriched amount of typical exosomal markers (e.g. CD63, CD81, CD9, TSG101, etc.) [96] and absence of potential contaminants such as organelles markers (e.g. calnexin, GM130, etc.) [97].

In our characterization we utilized a high-throughput quantitative protein profiling approach based on mass-spectrometry (MS). Briefly, aliquots containing 100 μg of each cell lysate (CL) sample and 30 μg of each EVs sample were digested with trypsin over night using the filter-aided sample preparation (FASP) method [98]. In order to reduce the sample complexity, each CL sample was run through a fractionation kit and eight fractions collected. The samples were then analyzed by liquid chromatography tandem mass spectrometry (LC-MS/MS) [99] using two quantitative methods, namely a) tandem mass tags (TMT)-based LC-MS/MS [100], and b) intensity-based absolute quantification (iBAQ) [101].

In summary, fractions were placed in an Easy-nLC 1000 nanoflow liquid chromatography system interfacing an Orbitrap Fusion Tribrid mass spectrometer (Thermo Fisher Scientific) in which the sample is injected directly after LC separation.

In the a) TMT based method, the samples were isotope-labelled and mixed prior elution in the nLC system. This allows performing quantitation of the same peptides present in each sample relative to the other samples, hence to obtain a relative quantitation of proteins after identification (Fig. 10).

The b) method, iBAQ, allows scoring the abundance of each protein relative to one another within the same sample. It is considered a pseudo absolute quantitative proteomics approach as it provides an estimate of abundance based on the measured and theoretical intensities.

By combining pseudo absolute intra-sample quantification with relative inter-sample quantification one can establish that some proteins are very (much or little) abundant in just one sample. This allows interpreting the differences (intensities ratios) better than by the TMT-based quantitation alone.

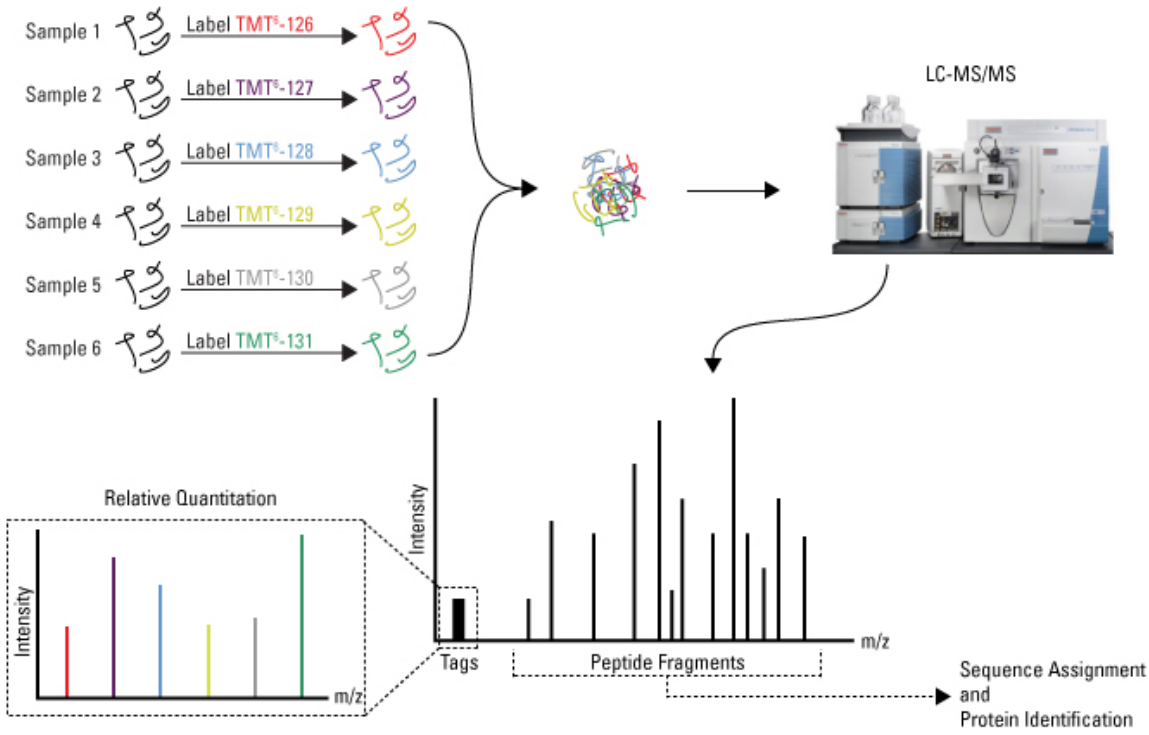

Figure 10 Schematic representation of multiplex proteomic quantitation. Samples are labeled with individual mass tags and then combined for LC-MS/MS analysis. Because the masses of all of the tags are the same, identical peptides from different samples co-elute and are analyzed by MS. After tag cleavage induced by higher energy collision dissociation (HCD) and another round of MS, the tags are used to quantitate relative peptide intensities, while the peptide fragment ions are sequenced for protein identification. (reproduced from https://www.thermofisher.com/se/en/home/life-science/protein-biology/protein-biology-learning-center/protein-biology-resource-library/pierce-protein-methods/quantitative-proteomics.html)

7.2 Lipidomics

The exosomal lipidome is not as well-studied as the proteome or the transcriptome. This is due to two main reasons which apply generally to lipidomics research beyond the extracellular vesicles field: 1) the bigger scale and higher complexity of the world of lipids; 2) the long-held idea that biological functions and diseases could be explained to the greatest extent by decoding the information at the gene and protein levels and their mutual interactions. It is interesting to stress that the known number of biologically relevant lipids grew exponentially in the recent years, from a mere 1000 cellular lipids [102] to over 40000 documented unique chemical structures in the LIPID MAPS database (www.lipidmaps.org/data/structure/index.html). Furthermore, in theory, it is estimated that there are approximately 180000 different lipid species [103]. Placing lipids in perspective, their multitude and diversity is overwhelming compared to the human proteome. The latter observations suggest lipids may play critical biological functions. The recently developed technologies, informatics tools and analysis pipelines aiming at dissecting lipid-protein interactions, lipid synthesis and the role of lipids in metabolic pathways in healthy and disease

states further contribute to confirm this hypothesis by making it possible to study lipid-membrane related processes in a more comprehensive manner, taking into account the simultaneous contribution of multiple components to biomolecular interactions [104]. As summarized further in this section, questions concerning exosomal lipids are slowly being addressed in the literature, not only in regard to the mere composition but also on the role of specific lipids and lipid-proteins interactions for the production and transfer of extracellular vesicles.

Lipids have for long been analyzed using chromatography techniques, which normally rely on one or more of the following characteristics: polarity, mass, solubility, and affinity. However, even the most advanced separation techniques don't allow a resolution beyond identification of different lipid classes. Mass spectrometry methods based on similar principles to those utilized in proteomics (see section 2.1) provide an alternative or can be used in combination with chromatography (e.g. high performance liquid chromatography mass spectrometry - HPLC-MS) and are essential nowadays for lipids profiling. Nonetheless, the high molecular heterogeneity of lipids is reflected in highly distributed and overlapping mass fingerprints, making identification and profiling a complex and massive task. Yet the field of lipidomics is expanding and technical improvements are slowly being achieved [105].

The few studies analyzing the lipid content of exosomes have shown that the levels of sphingomyelins, phosphatidylserines and phosphatidylinositols are increased compared to the cellular plasma membrane. Furthermore, phosphatidylcholines are less abundant [106]–[110]. While some studies have suggested that cholesterol is enriched in the exosomal membrane compared to the cellular membrane, [106], [108]–[110] others have reported no increase in the ratio between cholesterol and phospholipids in the exosomal membrane [107]. Generally speaking, the particular composition of the exosomal membrane is likely to reflect the biogenesis and affect uptake and interactions with cellular compartments. For instance, some showed that exosomes budding is triggered by ceramides and is not associated with the endosomal sorting complex required for transport (ESCRT) [111]; others found that inhibition of ceramide formation does not block exosomes secretion in PC-3 cells, while the raft-associated proteins, glycosphingolipids and flotillins affect the composition of released exosomes [112]. In the case of mesenchymal stem cells, exosome biogenesis has been associated with the presence of lipid rafts as expected for vesicles of endocytic origin [113]. These pioneering studies illustrate the importance of lipidomic investigations and it is likely that progress in the field will provide further valuable insights into exosome functions. A clearer picture of exosomal lipid composition may also result in useful methods for the discrimination of exosomes versus other lipid vesicles [114].

Chapter 8
Summary of results

In Paper I we illustrate a method to calculate the LSPR shifts of different nanosensor geometries. The method is based on the local field intensities of the different constituents of the interacting system. We show its accuracy in comparison to Finite Difference Time Domain (FDTD) simulations. Local sensitivity maps for various plasmonic sensors can be obtained.

In Paper II we use stochastic diffusion-reaction simulations to analyze the site dependent binding probability of diffusing molecules for various sensor geometries. We also compare the effect of inhomogeneous sensitivity distributions. The results are used to discuss the implications of these geometrical effects on the accuracy of the signal both in ensemble measurements and single-molecule observations. This system can further be used to study reaction rates in a quantitative way. For instance, the simulation of stochastic binding traces could test the relation between the reaction rates as calculated in solution and as accessible by single-molecule studies on surface sensors.

In Paper III an extensive review on the world of extracellular vesicles and exosomes is offered from the prospective of biophysical characterization. Methods for qualitative and quantitative analysis are illustrated with their advantages and limitations.

In Paper IV an extended formalism for the SPR response to films, rigid beads, and both deformed and undeformed vesicles was used to interpret dual-wavelength SPR measurements. In combination with complementary techniques (NTA, fluorescent NTA and TEM) the size of vesicles and exosomes was determined with high accuracy together with the degree of deformation upon binding of CD63 positive exosomes. Moreover, a better estimate of their bulk concentration as a sub-population of the total suspended exosomes was achieved.

In Paper V we characterized the content of EVs isolated from two commercial (U87 and H4) and two primary glioma lines. U87 and H4 were treated with either hypoxia or a chemical inducer of oxidative stress (tBHP), while the primary lines were treated only with tBHP. We performed quantitative proteomics, transcriptomics and lipidomics on EVs and total cell extracts in treated conditions versus control and also compare across cell types. We found that: i) the proteome changes due to stress after 24h are weak in CLs but relatively large in the EVs; ii) EVs are abundant in RNA-binding proteins; iii) the major differences among samples were attributable to the cell type rather than the types of stressor; iv) despite very similar proteome of the cell lysates and EVs from the primary cell lines with respect to the commercial lines, their response to oxidative stress in terms of EVs proteome was rather negatively correlated; v) the U87 cells and EVs were the least responsive in terms of protein and RNA changes; vi) the lipidome of U87 and H4 cells vs. exosomes is markedly different; vii) while the lipidome of cell extracts seemed to be noticeably cell-type dependent and somewhat affected by stress, the lipid composition of EVs across these variables was rather homogeneous and in contrast with the major proteomic changes.

Chapter 9
Outlook

Biophysical modeling and highly sensitive physical platforms such as dual wavelength SPR are great tools not only to optimize and push the limits of sensing when a sensor is highly heterogeneous, but also to enable the correct interpretation of ensemble measurements in advanced sensing experiments of complex biological samples. Further development of these biophysical approaches, coupled with better vesicle isolation procedures pave the way to more precise analysis and biological studies that are required to inform a fundamental understanding and shape a consensus in this field. Moreover, any advance in this direction may lead to clinically and commercially relevant detection schemes.

Specifically, in the case of EVs from glioblastoma, we have shown how their content changes strongly in response to stress and this change is cell-type dependent, in ways that are not easily predictable from broad similarities across cellular types. Primary cell lines that are also cancer stem cells have a distinct proteome and their EV content is markedly different from that of commercial cell lines. Studies found out that the U87 cell line, which has been considered for long a standard in cancer research should be reconsidered as it may have become a very artificial line far from real glioblastoma. If one wants to understand cellular communication in cancer in response to stimuli, a high number of primary cell lines [115] may be needed in the same study in order to tease out specific predictable differences that may be used in diagnostics or therapy.

One recurrent category of proteins in EV proteomics is that of RNA-binding proteins. These proteins may turn out to be an interesting target for further investigations in several directions. In fact, the function of RBPs in EV-mediated cellular communication is not clear. Some of these proteins appear, for instance, in DNA remodeling pathways, hence suggesting an epigenetic modification of the recipient cells that is yet to be explored. Also, deeper data-mining analysis, for instance using RNA binding domains (RBDs) and their target binding sequences, coupled to new experiments in the field of RNA molecules processing and transport, may help finding an explanation on how various RNAs are produced, packaged into exosomes and unpackaged in recipient cells. Of great interest in this regard is the approach and results obtained by combining quantitative proteomics, miRNA transcriptomics and in vitro vesicles production leading for example to the identification of YBX1 as preferential binding protein of the microRNA mi-223 and responsible for its loading into vesicles in cells and in cell-free assays [116]. Omics-based profiling of EVs could also reveal long-range and systemic communication in the healthy and diseased human body.

Physical measurements of EVs, in combination with biomolecular experiments, will additionally help shedding light on specific and general features. For instance, one study showed that heparanase stimulates the exosomal secretion of syntenin-1, syndecan and other exosomal markers, such as CD63, in a concentration-dependent manner. In contrast, exosomal CD9, CD81 and flotillin-1 were not affected [106]. In our dataset, we did not observe ALIX and syndecan, but we found all other markers mentioned (syntenin, CD63, CD9, CD81, CD82, flotillin). Vesicles from different cell lines can vary a lot in composition, but it is also plausible that some basic features are shared across a multitude of cell types of

origin. Hence, with methods and results presented in this thesis, one could design experiments to compare the size of different exosome batches and sub-populations. Further, by comparing for instance the same sub-populations derived from different cell types (e.g. by including the deformation and size distribution formalism in future dual-wavelength and other experiments) one might find out indicative information to answer, among others, questions on the composition and biogenesis of exosomes regardless of cell-type, or tease out important differences among EVs from the same cell type exposed to different stimuli.

Acknowledgments

First and foremost I would like to express my gratitude to my supervisor Georg Kuhn and to my examiner Fredrik Höök. Georg, thank you for accepting me in your lab and granting me a unique chance to explore the field of neuroscience. Your openness, curiosity and optimism were much appreciated, refreshing and encouraging. Fredrik, thank you for welcoming me in your group and allowing this extramural adventure. I appreciate you guiding my progress towards the end with a critical and supportive eye. It has been a great learning experience and an honor being exposed to and being a tiny part of both your passionate scientific endeavors.

I also wish to thank Julie Gold and Peter Apell for their co-supervision and guidance throughout this journey.

Here follows a list of collaborators whom I sincerely want to thank and acknowledge.
Tomasz Antosiewicz, for help with the simulations and the continued support and friendship.
Helena Carén, for accepting to collaborate and sharing precious primary cancer stem cells.
Jörg Hanrieder, for the great availability and expert collaboration in the lipidomics analysis.
Ágota Tűzesi, for the smooth and punctual collaboration, and the passion for research and exploration that one can read in your eyes.
Wojciech Mincho, for your work and motivation in performing the MALDI and prompt help figuring out how to extract valuable lipids information.
Deborah Rupert, for the interesting collaboration and all the tips on work-life balance.
Cecilia Lässer, for contributing to a steeper learning curve while writing the review.
Carina Sihlbom, Kanita Cukur and Egor Vorontsov at the Proteomics Core Facility at Sahlgrenska Academy for the great prolonged support for the proteomics in this thesis.
Katarina Tomazin, Kevin Weiss, Prince Nana Twum, Chesia Testa, Davide Lovera, Eva Brigos, for all your hard work, your questions, sharing frustrations and mistakes, putting up with frequent plan revisions and trouble-shooting, keeping me humble and motivated.
Marta Bally and Hudson Pace, for support and supervision with your expertise and for sharing the enthusiasm to try finding out if native membranes and exosomes interaction experiments can be done.

I further wish to thank and acknowledge all the scientists who exchanged their knowledge with me and provided answers when I contacted them virtually or in real life looking for help or advice. They are numerous, but here we go with those whose name my brain remembers:
Alexander Berezhkovskii at NIH/CIT, Maryland – for the lessons and insights on stochastic modeling of diffusion-controlled reactions.
Georgia Minakaki, Holger Meixner, Jochen Klucken, Jürgen Winkler – for welcoming me in Erlangen, sharing their expertise and ideas on exosomes and giving me valuable advice on my project at the start.
Nunzio Iraci – for help getting started with WBs of exosomal markers.
Klas Blomberg – for welcoming me at Karolinska Institute to attempt automated WBs.
Rastislav Horos and Matthias Hentze – answering questions on enigmRBPs.
Stefanie Gerstberger and Thomas Tuschl – help understanding their RBPs census.

Avi Maayan and Neil Clark – help understanding the use of R package for PAEA.
Gary Bader – help understanding Cytoscape 3.4 and GeneMANIA.
Barry Damchak – promptly fixed bug #3626: cPath and GeneMANIA.
Giulio Valentino Della Riva – crash course and help with R visualization packages.
Alain Brisson – answering on the impact of isolation methods on EVs quality.

And let me continue by whole-heartedly thanking:
Ann-Marie Alborn and Birgit Linder, the wonderful research technicians who introduced me to the cell lab and more, always helped me to find info, stuff or people and who glow in kindness all the time.
Reza Motalleb, Lars Karlsson and Olle Lindberg for contributing to a functioning lab, a nicely crowded office and an overall friendly and fun working atmosphere.
YanYan Sun, for her indefatigable smile and ready help anytime I asked.
Changlian and his group, for the nice occasions of cultural and scientific exchange.
Everyone at the Institute of Neuroscience, especially the students and postdocs on the 4th and S floor, for the fun environment.
Eric Hanse and the 3rd floor people, for the privileged opportunity to join the Friday journal club and for hosting me during the office and floor transfer.
Biological Physics, for being a unique friendly and fun bunch of passionate researchers.
Mokhtar Mapar, for being an inspiration as a colleague and as a friend in many ways.
Tomasz Antosiewicz, for the continued support and friendship.
Barbara D'Angelo, a rock in science and life, I am truly glad I got to know you.
All the engaged and passionate people I met in the representative bodies, particularly the Chalmers Doctoral Student Guild (Doktorandsektionen, DS) and the Association of Graduate Students in Physics (Föreningen för Forskarstuderande i Fysik, FFF). Thanks for making this journey more fun and meaningful.
Bengt Stebler and Moyra McDill, for their dedicated work as Ombudsman supporting PhD students across Chalmers.

Special thanks to my dearest supporters:
Giulia Zanni, a precious reference point in science and life, and a great sun substitute when you don't drag me to Mexico.
Per-Magnus, for the trust and comprehension, and for reminding me of the value of doing and giving in a "do *utan* des" fashion.
All the close and far away friends who kept me cheered up and made the dearest and most pleasant memories.
My life partner Björn, thank you for your immense and patient support, the long hauls and improbable adventures.
My precious family, whose care and love know no limits, grazie infinite!

References

[1] "NIH Guide: SINGLE MOLECULE DETECTION AND MANIPULATION," 2001. [Online]. Available: http://grants.nih.gov/grants/guide/pa-files/PA-01-050.html.

[2] A. A. Deniz, S. Mukhopadhyay, and E. A. Lemke, "Single-molecule biophysics: at the interface of biology, physics and chemistry," *J. R. Soc. Interface* , vol. 5, no. 18, pp. 15–45, Jan. 2008.

[3] I. Tinoco and R. L. Gonzalez, "Biological mechanisms, one molecule at a time," *Genes Dev.* , vol. 25, no. 12, pp. 1205–1231, Jun. 2011.

[4] M. Coelho, N. Maghelli, and I. M. Tolic-Norrelykke, "Single-molecule imaging in vivo: the dancing building blocks of the cell," *Integr. Biol.*, 2013.

[5] Y. Sako and T. Yanagida, "Single-molecule visualization in cell biology.," *Nat. Rev. Mol. Cell Biol.*, vol. Suppl, no. September, p. SS1-5, Oct. 2003.

[6] D. R. Walt, "Optical methods for single molecule detection and analysis.," *Anal. Chem.*, vol. 85, no. 3, pp. 1258–63, Mar. 2013.

[7] Y. Pang and R. Gordon, "Optical trapping of a single protein.," *Nano Lett.*, vol. 12, no. 1, pp. 402–6, Jan. 2012.

[8] M. J. Comstock, T. Ha, and Y. R. Chemla, "Ultrahigh-resolution optical trap with single-fluorophore sensitivity.," *Nat. Methods*, vol. 8, no. 4, pp. 335–40, Apr. 2011.

[9] D. P. Malinowski, "Molecular diagnostic assays for cervical neoplasia: emerging markers for the detection of high-grade cervical disease.," *Biotechniques*, vol. Suppl, pp. 17–23, May 2005.

[10] M. Hintersteiner and M. Auer, "Single-bead, single-molecule, single-cell fluorescence: technologies for drug screening and target validation.," *Ann. N. Y. Acad. Sci.*, vol. 1130, no. 2008, pp. 1–11, Jan. 2008.

[11] G. M. Skinner and K. Visscher, "Single-molecule techniques for drug discovery.," *Assay Drug Dev. Technol.*, vol. 2, no. 4, pp. 397–405, Aug. 2004.

[12] M. L. Goodenberger and R. B. Jenkins, "Genetics of adult glioma," *Cancer Genet.*, vol. 205, no. 12, pp. 613–621, May 2017.

[13] "Glioblastoma (GBM)," *American Brain Tumor Association*. [Online]. Available: http://www.abta.org/brain-tumor-information/types-of-tumors/glioblastoma.html.

[14] H. Clevers, "The cancer stem cell: premises, promises and challenges.," *Nat. Med.*, vol. 17, no. 3, pp. 313–9, 2011.

[15] T. N. Ignatova, V. G. Kukekov, E. D. Laywell, O. N. Suslov, F. D. Vrionis, and D. A. Steindler, "Human cortical glial tumors contain neural stem-like cells expressing astroglial and neuronal markers in vitro," *Glia*, vol. 39, no. 3, pp. 193–206, 2002.

[16] H. Carén, S. M. Pollard, and S. Beck, "The good, the bad and the ugly: Epigenetic mechanisms in glioblastoma," *Mol. Aspects Med.*, vol. 34, no. 4, pp. 849–862, 2013.

[17] J. Lee, S. Kotliarova, Y. Kotliarov, A. Li, Q. Su, N. M. Donin, S. Pastorino, B. W. Purow, N. Christopher, W. Zhang, J. K. Park, and H. A. Fine, "Tumor stem cells derived from glioblastomas cultured in bFGF and EGF more closely mirror the phenotype and genotype of primary tumors than do serum-cultured cell lines," *Cancer Cell*, vol. 9, no. 5, pp. 391–403, May 2017.

[18] M. Allen, M. Bjerke, H. Edlund, S. Nelander, and B. Westermark, "Origin of the

U87MG glioma cell line : Good news and bad news," *Sci. Transl. Med.*, vol. 354, no. 8, pp. 1–4, 2016.

[19] P. Kharaziha, S. Ceder, Q. Li, and T. Panaretakis, "Tumor cell-derived exosomes: A message in a bottle," *Biochim. Biophys. Acta - Rev. Cancer*, vol. 1826, no. 1, pp. 103–111, 2012.

[20] I. Tatischeff, "Cell-derived Extracellular Vesicles Open New Perspectives for Cancer Research," *Cancer Res. Front.*, vol. 1, no. 2, pp. 208–224, 2015.

[21] M. W. Graner, O. Alzate, A. M. Dechkovskaia, J. D. Keene, J. H. Sampson, D. A. Mitchell, and D. D. Bigner, "Proteomic and immunologic analyses of brain tumor exosomes," *FASEB J.*, vol. 23, no. 5, pp. 1541–1557, May 2009.

[22] J. Skog, T. Würdinger, S. van Rijn, D. H. Meijer, L. Gainche, M. Sena-Esteves, W. T. Curry, B. S. Carter, A. M. Krichevsky, and X. O. Breakefield, "Glioblastoma microvesicles transport RNA and proteins that promote tumour growth and provide diagnostic biomarkers.," *Nat. Cell Biol.*, vol. 10, no. 12, pp. 1470–6, Dec. 2008.

[23] K. J. Svensson, P. Kucharzewska, H. C. Christianson, S. Sköld, T. Löfstedt, M. C. Johansson, M. Mörgelin, J. Bengzon, W. Ruf, and M. Belting, "Hypoxia triggers a proangiogenic pathway involving cancer cell microvesicles and PAR-2-mediated heparin-binding EGF signaling in endothelial cells.," *Proc. Natl. Acad. Sci. U. S. A.*, vol. 108, no. 32, pp. 13147–52, 2011.

[24] P. Kucharzewska, H. C. Christianson, J. E. Welch, K. J. Svensson, E. Fredlund, M. Ringnér, M. Mörgelin, E. Bourseau-Guilmain, J. Bengzon, and M. Belting, "Exosomes reflect the hypoxic status of glioma cells and mediate hypoxia-dependent activation of vascular cells during tumor development.," *Proc. Natl. Acad. Sci. U. S. A.*, vol. 110, no. 18, pp. 7312–7, 2013.

[25] K. Jelonek, A. Wojakowska, L. Marczak, A. Muer, I. Tinhofer-Keilholz, M. Lysek-Gladysinska, P. Widlak, and M. Pietrowska, "Ionizing radiation affects protein composition of exosomes secreted in vitro from head and neck squamous cell carcinoma," *Acta Biochim. Pol.*, vol. 62, no. 2, pp. 265–272, 2015.

[26] S. N. Thomas, Z. Liao, D. Clark, Y. Chen, R. Samadani, L. Mao, D. K. Ann, J. E. Baulch, P. Shapiro, and A. J. Yang, "Exosomal Proteome Profiling: A Potential Multi-Marker Cellular Phenotyping Tool to Characterize Hypoxia-Induced Radiation Resistance in Breast Cancer," *Proteomes*, vol. 1, no. 2, pp. 87–108, 2013.

[27] P. J. Kallio, W. J. Wilson, S. O'Brien, Y. Makino, and L. Poellinger, "Regulation of the hypoxia-inducible transcription factor 1?? by the ubiquitin-proteasome pathway," *J. Biol. Chem.*, vol. 274, no. 10, pp. 6519–6525, 1999.

[28] D. Zagzag, Y. Lukyanov, L. Lan, M. A. Ali, M. Esencay, O. Mendez, H. Yee, E. B. Voura, and E. W. Newcomb, "Hypoxia-inducible factor 1 and VEGF upregulate CXCR4 in glioblastoma: implications for angiogenesis and glioma cell invasion.," *Lab. Invest.*, vol. 86, no. 12, pp. 1221–1232, 2006.

[29] M. K. Bates, "Culturing Cells Under Hypoxic Conditions for Biologically Relevant Results," *Am. Lab.*, no. October, pp. 1–3, 2012.

[30] L. A. Shimoda, "55th Bowditch Lecture: Effects of chronic hypoxia on the pulmonary circulation: Role of HIF-1," *J. Appl. Physiol.*, vol. 113, no. 9, p. 1343 LP-1352, Nov. 2012.

[31] K. Vandenbroucke, S. Robbens, K. Vandepoele, D. Inzé, Y. Van De Peer, and F. Van Breusegem, "Hydrogen peroxide-induced gene expression across kingdoms: A

comparative analysis," *Mol. Biol. Evol.*, vol. 25, no. 3, pp. 507–516, 2008.

[32] C. Vogel, G. M. Silva, and E. M. Marcotte, "Protein Expression Regulation under Oxidative Stress," *Mol. Cell. Proteomics*, vol. 10, no. 12, p. M111.009217, Dec. 2011.

[33] J. D. Morrow, K. E. Hill, R. F. Burk, T. M. Nammour, K. F. Badr, and L. J. Roberts, "A series of prostaglandin F2-like compounds are produced in vivo in humans by a non-cyclooxygenase, free radical-catalyzed mechanism.," *Proc. Natl. Acad. Sci. U. S. A.*, vol. 87, no. 23, pp. 9383–9387, 1990.

[34] K. B. Jourdan, T. W. Evans, P. Goldstraw, and J. a Mitchell, "Isoprostanes and PGE2 production in human isolated pulmonary artery smooth muscle cells: concomitant and differential release.," *FASEB J.*, vol. 13, no. 9, pp. 1025–30, 1999.

[35] T. R. International, "Tert-Butyl hydroperoxide," pp. 1–33, 2001.

[36] K. S. Hwang, S.-M. Lee, S. K. Kim, J. H. Lee, and T. S. Kim, "Micro- and nanocantilever devices and systems for biomolecule detection.," *Annu. Rev. Anal. Chem. (Palo Alto. Calif).*, vol. 2, pp. 77–98, Jan. 2009.

[37] G. Zheng, F. Patolsky, Y. Cui, W. U. Wang, and C. M. Lieber, "Multiplexed electrical detection of cancer markers with nanowire sensor arrays," *Nat Biotech*, vol. 23, no. 10, pp. 1294–1301, Oct. 2005.

[38] F. Patolsky and C. M. Lieber, "Nanowire nanosensors," *Mater. Today*, vol. 8, no. 4, pp. 20–28, Apr. 2005.

[39] D. J. Bornhop, J. C. Latham, A. Kussrow, D. A. Markov, R. D. Jones, and H. S. Sorensen, "Free-Solution, Label-Free Molecular Interactions Studied by Back-Scattering Interferometry," *Science (80-.).*, vol. 317, no. 5845, pp. 1732–1736, Sep. 2007.

[40] K. A. Willets and R. P. Van Duyne, "Localized Surface Plasmon Resonance Spectroscopy and Sensing," *Annu. Rev. Phys. Chem.*, vol. 58, no. 1, pp. 267–297, Apr. 2007.

[41] R. L. Rich and D. G. Myszka, "Survey of the 2009 commercial optical biosensor literature," *J. Mol. Recognit.*, vol. 24, no. 6, pp. 892–914, 2011.

[42] X. Fan, I. M. White, S. I. Shopova, H. Zhu, J. D. Suter, and Y. Sun, "Sensitive optical biosensors for unlabeled targets: A review," *Anal. Chim. Acta*, vol. 620, no. 1–2, pp. 8–26, Jul. 2008.

[43] G. Gauglitz, "Direct optical sensors: principles and selected applications," *Anal. Bioanal. Chem.*, vol. 381, no. 1, pp. 141–155, 2005.

[44] D. B. Hibbert, J. J. Gooding, and P. Erokhin, "Kinetics of Irreversible Adsorption with Diffusion: Application to Biomolecule Immobilization," *Langmuir*, vol. 18, no. 5, pp. 1770–1776, Feb. 2002.

[45] T. M. Squires, R. J. Messinger, and S. R. Manalis, "Making it stick: convection, reaction and diffusion in surface-based biosensors.," *Nat. Biotechnol.*, vol. 26, no. 4, pp. 417–26, Apr. 2008.

[46] P. E. Sheehan and L. J. Whitman, "Detection limits for nanoscale biosensors.," *Nano Lett.*, vol. 5, no. 4, pp. 803–7, Apr. 2005.

[47] A. J. Haes and R. P. Van Duyne, "A Nanoscale Optical Biosensor: Sensitivity and Selectivity of an Approach Based on the Localized Surface Plasmon Resonance Spectroscopy of Triangular Silver Nanoparticles," *J. Am. Chem. Soc.*, vol. 124, no. 35,

pp. 10596–10604, Aug. 2002.

[48] J. C. Riboh, A. J. Haes, A. D. McFarland, C. Ranjit Yonzon, and R. P. Van Duyne, "A Nanoscale Optical Biosensor: Real-Time Immunoassay in Physiological Buffer Enabled by Improved Nanoparticle Adhesion," *J. Phys. Chem. B*, vol. 107, no. 8, pp. 1772–1780, Jan. 2003.

[49] A. M. Armani, R. P. Kulkarni, S. E. Fraser, R. C. Flagan, and K. J. Vahala, "Label-free, single-molecule detection with optical microcavities.," *Science*, vol. 317, no. 5839, pp. 783–7, Aug. 2007.

[50] S. Chen, M. Svedendahl, R. P. Van Duyne, and M. Käll, "Plasmon-enhanced colorimetric ELISA with single molecule sensitivity.," *Nano Lett.*, vol. 11, no. 4, pp. 1826–30, Apr. 2011.

[51] B. Liedberg, C. Nylander, and I. Lunström, "Surface plasmon resonance for gas detection and biosensing," *Sensors and Actuators*, vol. 4, no. 0, pp. 299–304, 1983.

[52] M. Rodahl, F. Hook, A. Krozer, P. Brzezinski, and B. Kasemo, "Quartz crystal microbalance setup for frequency and Q-factor measurements in gaseous and liquid environments," *Rev. Sci. Instrum.*, vol. 66, no. 7, pp. 3924–3930, Jul. 1995.

[53] R. L. Rich and D. G. Myszka, "Higher-throughput, label-free, real-time molecular interaction analysis.," *Anal. Biochem.*, vol. 361, no. 1, pp. 1–6, Feb. 2007.

[54] T. Bravman, V. Bronner, O. Nahshol, and G. Schreiber, "The ProteOn XPR36^{TM} Array System—High Throughput Kinetic Binding Analysis of Biomolecular Interactions," *Cell. Mol. Bioeng.*, vol. 1, no. 4, pp. 216–228, 2008.

[55] R. M. Lequin, "Enzyme immunoassay (EIA)/enzyme-linked immunosorbent assay (ELISA).," *Clin. Chem.*, vol. 51, no. 12, pp. 2415–8, Dec. 2005.

[56] E. Lüthgens and A. Janshoff, "Equilibrium coverage fluctuations: a new approach to quantify reversible adsorption of proteins.," *Chemphyschem*, vol. 6, no. 3, pp. 444–8, Mar. 2005.

[57] K. M. Mayer, F. Hao, S. Lee, P. Nordlander, and J. H. Hafner, "A single molecule immunoassay by localized surface plasmon resonance.," *Nanotechnology*, vol. 21, no. 25, p. 255503, Jun. 2010.

[58] T. Sannomiya, C. Hafner, and J. Voros, "In situ sensing of single binding events by localized surface plasmon resonance.," *Nano Lett.*, vol. 8, no. 10, pp. 3450–5, Oct. 2008.

[59] I. Ament, J. Prasad, A. Henkel, S. Schmachtel, and C. Sönnichsen, "Single Unlabeled Protein Detection on Individual Plasmonic Nanoparticles," *Nano Lett.*, vol. 12, no. 2, pp. 1092–1095, Jan. 2012.

[60] J.-H. Ahn, J.-H. Kim, N. F. Reuel, P. W. Barone, A. A. Boghossian, J. Zhang, H. Yoon, A. C. Chang, A. J. Hilmer, and M. S. Strano, "Label-free, single protein detection on a near-infrared fluorescent single-walled carbon nanotube/protein microarray fabricated by cell-free synthesis.," *Nano Lett.*, vol. 11, no. 7, pp. 2743–52, Jul. 2011.

[61] P. Zijlstra, P. M. R. Paulo, and M. Orrit, "Optical detection of single non-absorbing molecules using the surface plasmon resonance of a gold nanorod," *Nat Nano*, vol. 7, no. 6, pp. 379–382, Jun. 2012.

[62] D. Rupert, V. Claudio, C. Lässer, and M. Bally, "Methods for the physical characterization and quantification of extracellular vesicles in biological samples,"

Biochim. Biophys. Acta - Gen. Subj., 2016.

[63] G. G. N. and M. P. and J. Homola, "Data analysis for optical sensors based on spectroscopy of surface plasmons," *Meas. Sci. Technol.*, vol. 13, no. 12, p. 2038, 2002.

[64] X. Wang, M. Jefferson, P. C. D. Hobbs, W. P. Risk, B. E. Feller, R. D. Miller, and A. Knoesen, "Shot-noise limited detection for surface plasmon sensing.," *Opt. Express*, vol. 19, no. 1, pp. 107–17, Jan. 2011.

[65] A. B. Dahlin, J. O. Tegenfeldt, and F. Höök, "Improving the Instrumental Resolution of Sensors Based on Localized Surface Plasmon Resonance," *Anal. Chem.*, vol. 78, no. 13, pp. 4416–4423, May 2006.

[66] T. Sannomiya, C. Hafner, and J. Vörös, "Shape-dependent sensitivity of single plasmonic nanoparticles for biosensing.," *J. Biomed. Opt.*, vol. 14, no. 6, p. 64027, 2011.

[67] A. Unger, U. Rietzler, R. Berger, and M. Kreiter, "Sensitivity of crescent-shaped metal nanoparticles to attachment of dielectric colloids.," *Nano Lett.*, vol. 9, no. 6, pp. 2311–5, Jun. 2009.

[68] H. Cang, A. Labno, C. Lu, X. Yin, M. Liu, C. Gladden, Y. Liu, and X. Zhang, "Probing the electromagnetic field of a 15-nanometre hotspot by single molecule imaging.," *Nature*, vol. 469, no. 7330, pp. 385–8, Jan. 2011.

[69] E. C. Le Ru, P. G. Etchegoin, and M. Meyer, "Enhancement factor distribution around a single surface-enhanced Raman scattering hot spot and its relation to single molecule detection.," *J. Chem. Phys.*, vol. 125, no. 20, p. 204701, Nov. 2006.

[70] P. G. Etchegoin, M. Meyer, and E. C. Le Ru, "Statistics of single molecule SERS signals: is there a Poisson distribution of intensities?," *Phys. Chem. Chem. Phys.*, vol. 9, no. 23, pp. 3006–10, Jun. 2007.

[71] S. Maier, *Plasmonics: Fundamentals and Applications*. Springer New York, 2007.

[72] P. Drude, *No Title*. Leipzig: Hirzel, 1900.

[73] E. Kretschmann and R. Raether, "Radiative decay of nonradiative surface plasmons excited by light," *Z. Naturforsch. A*, vol. 23, pp. 2135–2136, 1968.

[74] L. S. Jung, C. T. Campbell, T. M. Chinowsky, M. N. Mar, and S. S. Yee, "Quantitative Interpretation of the Response of Surface Plasmon Resonance Sensors to Adsorbed Films," *Langmuir*, vol. 14, no. 19, pp. 5636–5648, 1998.

[75] S. Sjoelander and C. Urbaniczky, "Integrated fluid handling system for biomolecular interaction analysis," *Anal. Chem.*, vol. 63, no. 20, pp. 2338–2345, Oct. 1991.

[76] D. L. M. Rupert, C. Lässer, M. Eldh, S. Block, V. P. Zhdanov, J. Lotvall, M. Bally, and F. Höök, "Determination of exosome concentration in solution using surface plasmon resonance spectroscopy.," *Anal. Chem.*, vol. 86, pp. 5929–5936, 2014.

[77] M. Svedendahl, S. Chen, A. Dmitriev, and M. Käll, "Refractometric sensing using propagating versus localized surface plasmons: a direct comparison.," *Nano Lett.*, vol. 9, no. 12, pp. 4428–33, Dec. 2009.

[78] B. T. Draine and P. J. Flatau, "Discrete-dipole approximation for scattering calculations," *J. Opt. Soc. Am. A*, vol. 11, no. 4, p. 1491, Apr. 1994.

[79] R. Huang, I. Chavez, K. M. Taute, B. Lukic, S. Jeney, M. G. Raizen, and E.-L. Florin, "Direct observation of the full transition from ballistic to diffusive Brownian motion in a liquid," *Nat Phys*, vol. 7, no. 7, pp. 576–580, Jul. 2011.

[80] M. V. Smoluchowski, “Versuch einer mathematischen Theorie der Koagulationskinetik kolloider Lösungen,” *z. Phys. Chem.*, vol. 92, p. 129, 1917.

[81] F. C. Collins and G. E. Kimball, “Diffusion-controlled reaction rates,” *J. Colloid. Sci.*, vol. 4, pp. 425–437, 1949.

[82] D. T. Gillespie, “A general method for numerically simulating the stochastic time evolution of coupled chemical reactions,” *J. Comput. Phys.*, vol. 22, no. 4, pp. 403–434, Dec. 1976.

[83] D. T. Gillespie, “Stochastic simulation of chemical kinetics.,” *Annu. Rev. Phys. Chem.*, vol. 58, pp. 35–55, Jan. 2007.

[84] R. Erban and S. J. Chapman, “Stochastic modelling of reaction-diffusion processes: algorithms for bimolecular reactions.,” *Phys. Biol.*, vol. 6, no. 4, p. 46001, Jan. 2009.

[85] S. S. Andrews and D. Bray, “Stochastic simulation of chemical reactions with spatial resolution and single molecule detail.,” *Phys. Biol.*, vol. 1, no. 3–4, pp. 137–51, Dec. 2004.

[86] A. Mahmutovic, D. Fange, O. G. Berg, and J. Elf, “Lost in presumption: stochastic reactions in spatial models,” *Nat Meth*, vol. 9, no. 12, pp. 1163–1166, Dec. 2012.

[87] A. a. Boghossian, J. Zhang, F. T. Le Floch-Yin, Z. W. Ulissi, P. Bojo, J.-H. Han, J.-H. Kim, J. R. Arkalgud, N. F. Reuel, R. D. Braatz, and M. S. Strano, “The chemical dynamics of nanosensors capable of single-molecule detection,” *J. Chem. Phys.*, vol. 135, no. 8, p. 84124, 2011.

[88] C. Versari, “A Core Calculus for a Comparative Analysis of Bio-inspired Calculi,” in *Programming Languages and Systems SE - 28*, vol. 4421, R. Nicola, Ed. Springer Berlin Heidelberg, 2007, pp. 411–425.

[89] G. E. P. Box and M. E. Muller, “A note on the generation of random normal deviates,” *Ann. Math. Stat.*, vol. 29, pp. 610–611, 1958.

[90] H. C. Berg, *Random Walks in Biology*, 1993rd ed. Princeton: Princeton University Press, 1983.

[91] I. Ezkurdia, D. Juan, J. M. Rodriguez, A. Frankish, M. Diekhans, J. Harrow, J. Vazquez, A. Valencia, and M. L. Tress, “Multiple evidence strands suggest that there may be as few as 19 000 human protein-coding genes,” *Hum. Mol. Genet.*, vol. 23, no. 22, pp. 5866–5878, Nov. 2014.

[92] L. Breuza, S. Poux, A. Estreicher, M. L. Famiglietti, M. Magrane, M. Tognolli, A. Bridge, D. Baratin, and N. Redaschi, “The UniProtKB guide to the human proteome,” *Database*, vol. 2016, p. bav120-bav120, Jan. 2016.

[93] “UniProt: the universal protein knowledgebase,” *Nucleic Acids Res.*, vol. 45, no. D1, pp. D158–D169, Jan. 2017.

[94] M. Baker, “Blame it on the Antibodies,” *Nature*, vol. 521, pp. 274–275, 2015.

[95] M. G. Weller, “Quality Issues of Research Antibodies,” *Anal. Chem. Insights*, vol. 11, pp. 21–27, Mar. 2016.

[96] S. Keerthikumar, D. Chisanga, D. Ariyaratne, H. Al Saffar, S. Anand, K. Zhao, M. Samuel, M. Pathan, M. Jois, N. Chilamkurti, L. Gangoda, and S. Mathivanan, “ExoCarta: A Web-Based Compendium of Exosomal Cargo,” 2016.

[97] J. Lötvall, A. F. Hill, F. Hochberg, E. I. Buzás, D. Di Vizio, C. Gardiner, Y. S. Gho, I. V Kurochkin, S. Mathivanan, P. Quesenberry, S. Sahoo, H. Tahara, M. H. Wauben, K.

W. Witwer, and C. Théry, “Minimal experimental requirements for definition of extracellular vesicles and their functions: a position statement from the International Society for Extracellular Vesicles,” *J. Extracell. Vesicles*, vol. 3, p. 10.3402/jev.v3.26913, Dec. 2014.

[98] J. R. Wisniewski, A. Zougman, N. Nagaraj, and M. Mann, “Universal sample preparation method for proteome analysis,” *Nat. Meth.*, vol. 6, no. 5, pp. 359–362, 2009.

[99] J. Peng, J. E. Elias, C. C. Thoreen, L. J. Licklider, and S. P. Gygi, “Evaluation of Multidimensional Chromatography Coupled with Tandem Mass Spectrometry (LC/LC−MS/MS) for Large-Scale Protein Analysis: The Yeast Proteome,” *J. Proteome Res.*, vol. 2, no. 1, pp. 43–50, Feb. 2003.

[100] A. Thompson, J. Schäfer, K. Kuhn, S. Kienle, J. Schwarz, G. Schmidt, T. Neumann, and C. Hamon, “Tandem Mass Tags: A Novel Quantification Strategy for Comparative Analysis of Complex Protein Mixtures by MS/MS,” *Anal. Chem.*, vol. 75, no. 8, pp. 1895–1904, Apr. 2003.

[101] B. Schwanhausser, D. Busse, N. Li, G. Dittmar, J. Schuchhardt, J. Wolf, W. Chen, and M. Selbach, “Global quantification of mammalian gene expression control,” *Nature*, vol. 473, no. 7347, pp. 337–342, 2011.

[102] G. van Meer, “Cellular lipidomics,” *EMBO J.*, vol. 24, no. 18, pp. 3159–3165, 2005.

[103] B. Brügger, “Lipidomics: analysis of the lipid composition of cells and subcellular organelles by electrospray ionization mass spectrometry.,” *Annu. Rev. Biochem.*, vol. 83, pp. 79–98, 2014.

[104] A. Shevchenko and K. Simons, “Lipidomics: coming to grips with lipid diversity,” *Nat Rev Mol Cell Biol*, vol. 11, no. 8, pp. 593–598, Aug. 2010.

[105] H. C. Köfeler, A. Fauland, G. N. Rechberger, and M. Trötzmüller, “Mass Spectrometry Based Lipidomics: An Overview of Technological Platforms,” *Metabolites*, vol. 2, no. 1, pp. 19–38, Mar. 2012.

[106] M. Vidal, J. Sainte-Marie, J. R. Philippot, and A. Bienvenue, “Asymmetric distribution of phospholipids in the membrane of vesicles released during in vitro maturation of guinea pig reticulocytes: Evidence precluding a role for ‘aminophospholipid translocase,’” *J. Cell. Physiol.*, vol. 140, no. 3, pp. 455–462, 1989.

[107] K. Laulagnier, C. Motta, S. Hamdi, S. Roy, F. Fauvelle, J.-F. Pageaux, T. Kobayashi, J.-P. Salles, B. Perret, C. Bonnerot, and M. Record, “Mast cell- and dendritic cell-derived exosomes display a specific lipid composition and an unusual membrane organization.,” *Biochem. J.*, vol. 380, no. Pt 1, pp. 161–71, 2004.

[108] A. Llorente, T. Skotland, T. Sylvänne, D. Kauhanen, T. Róg, A. Orłowski, I. Vattulainen, K. Ekroos, and K. Sandvig, “Molecular lipidomics of exosomes released by PC-3 prostate cancer cells,” *Biochim. Biophys. Acta - Mol. Cell Biol. Lipids*, vol. 1831, no. 7, pp. 1302–1309, 2013.

[109] I. Parolini, C. Federici, C. Raggi, L. Lugini, S. Palleschi, A. De Milito, C. Coscia, E. Iessi, M. Logozzi, A. Molinari, M. Colone, M. Tatti, M. Sargiacomo, and S. Fais, “Microenvironmental pH is a key factor for exosome traffic in tumor cells,” *J. Biol. Chem.*, vol. 284, no. 49, pp. 34211–34222, 2009.

[110] R. Wubbolts, R. S. Leckie, P. T. M. Veenhuizen, G. Schwarzmann, W. Möbius, J. Hoernschemeyer, J. W. Slot, H. J. Geuze, and W. Stoorvogel, “Proteomic and biochemical analyses of human B cell-derived exosomes: Potential implications for

their function and multivesicular body formation," *J. Biol. Chem.*, vol. 278, no. 13, pp. 10963–10972, 2003.

[111] K. Trajkovic, C. Hsu, S. Chiantia, L. Rajendran, D. Wenzel, F. Wieland, P. Schwille, B. Brügger, and M. Simons, "Ceramide triggers budding of exosome vesicles into multivesicular endosomes.," *Science*, vol. 319, no. April, pp. 1244–1247, 2008.

[112] S. Phuyal, N. P. Hessvik, T. Skotland, K. Sandvig, and A. Llorente, "Regulation of exosome release by glycosphingolipids and flotillins," *FEBS J.*, vol. 281, no. 9, pp. 2214–2227, 2014.

[113] S. S. Tan, Y. Yin, T. Lee, R. C. Lai, R. W. Y. Yeo, B. Zhang, A. Choo, S. K. Lim, R. Wee, Y. Yeo, B. Zhang, A. Choo, and S. K. Lim, "Therapeutic MSC exosomes are derived from lipid raft microdomains in the plasma membrane," *J. Extracell. vesicles*, vol. 2, no. 2, p. 22614, 2013.

[114] N. Kastelowitz and H. Yin, "Exosomes and microvesicles: Identification and targeting by particle size and lipid chemical probes," *ChemBioChem*, vol. 15, no. 7, pp. 923–928, 2014.

[115] Y. Xie, T. Bergström, Y. Jiang, P. Johansson, V. D. Marinescu, N. Lindberg, A. Segerman, G. Wicher, M. Niklasson, S. Baskaran, S. Sreedharan, I. Everlien, M. Kastemar, A. Hermansson, L. Elfineh, S. Libard, E. C. Holland, G. Hesselager, I. Alafuzoff, B. Westermark, S. Nelander, K. Forsberg-Nilsson, and L. Uhrbom, "The Human Glioblastoma Cell Culture Resource: Validated Cell Models Representing All Molecular Subtypes," *EBioMedicine*, vol. 2, no. 10, pp. 1351–1363, Oct. 2015.

[116] M. Shurtleff, K. V. Karfilis, M. Temoche-Diaz, S. Ri, and R. Schekman, "Y-box protein 1 is required to sort microRNAs into exosomes in cells and in a cell-free reaction," *bioRxiv*, p. 40238, 2016.

[117] H. C. Christianson, K. J. Svensson, T. H. van Kuppevelt, J.-P. Li, and M. Belting, "Cancer cell exosomes depend on cell-surface heparan sulfate proteoglycans for their internalization and functional activity.," *Proc. Natl. Acad. Sci. U. S. A.*, vol. 110, no. 43, pp. 17380–5, 2013.

[118] B. Roucourt, S. Meeussen, J. Bao, P. Zimmermann, and G. David, "Heparanase activates the syndecan-syntenin-ALIX exosome pathway.," *Cell Res.*, vol. 25, no. 4, pp. 412–28, 2015.